frontiers | Frontiers in Astronomy and Space Sciences

TYPE Methods
PUBLISHED 23 June 2023
DOI 10.3389/fspas.2023.1163517

OPEN ACCESS

EDITED BY
Benoit Lavraud,
UMR5804 Laboratoire d'astrophysique de Bordeaux (LAB), France

REVIEWED BY
Silvano Fineschi,
Osservatorio Astrofisico di Torino (INAF), Italy
Raphael Rougeot,
European Space Research and Technology Center (ESTEC), Netherlands

*CORRESPONDENCE
John F. Cooper,
cosmos.mariner.sav@gmail.com

RECEIVED 10 February 2023
ACCEPTED 02 June 2023
PUBLISHED 23 June 2023

CITATION
Cooper JF, Habbal SR, Boe B, Angelopoulos V, Sibeck DG, Paschalidis N, Sittler EC Jr., Jian LK and Killen RM (2023), Lunar Solar Occultation Explorer (LunaSOX).
Front. Astron. Space Sci. 10:1163517.
doi: 10.3389/fspas.2023.1163517

Lunar Solar Occultation Explorer (LunaSOX)

John F. Cooper[1]*, Shadia R. Habbal[2], Benjamin Boe[2], Vassilis Angelopoulos[3], David G. Sibeck[4], Nikolaos Paschalidis[4], Edward C. Sittler Jr.[4], Lan K. Jian[5] and Rosemary M. Killen[6]

[1]Emeritus, Heliospheric Physics Laboratory, Heliophysics Science Division, NASA Goddard Space Flight Center, Greenbelt, MD, United States, [2]Institute for Astronomy, University of Hawaii at Manoa, Honolulu, HI, United States, [3]Space Physics Center, Institute of Geophysics and Planetary Physics, University of California at Los Angeles, Los Angeles, CA, United States, [4]Geospace Physics Laboratory, Heliophysics Science Division, NASA Goddard Space Flight Center, Greenbelt, MD, United States, [5]Heliospheric Physics Laboratory, Heliophysics Science Division, NASA Goddard Space Flight Center, Greenbelt, MD, United States, [6]Planetary Magnetospheres Laboratory, Solar System Exploration Division, NASA Goddard Space Flight Center, Greenbelt, MD, United States

In the present decade and beyond, now 51 years after the last Apollo landing, the NASA Artemis human exploration program will offer abundant opportunities for heliophysics investigations from, by, and of the Moon from the vantage points of the lunar orbit and the surface. The Lunar Solar Occultation Explorer (LunaSOX) concept uses the lunar limb to occult the solar disk for high-resolution coronal observations at hourly, daily, to biweekly cadences from spacecraft either in the lunar orbit or at the surface. A 0.2 m diameter solar telescope in orbit with white light and narrow-band visible filters would provide arcsecond spectroscopic imaging of the low-to-high corona (1–10 R$\odot$) with an upper limit of 10^{-12} B$\odot$ on the local scattered light background from lunar atmospheric dust, as compared to 10^{-9} B$\odot$ for Earth ground-based solar eclipse observations looking up through the atmosphere at totality. For eclipse observations from and by the Moon, there would be no significant atmospheric disturbances that otherwise limit seeing to arcsec resolution from Earth's surface. The present eccentric orbits of the ARTEMIS P1 and P2 spacecraft are used as models for a 1 × 10 Rm orbit of LunaSOX to compute the times of solar eclipse intervals, up to 2 hours in duration between the east and west solar hemispheres at a daily cadence for coronal observations at 1–16 R$\odot$ when the orbital aposelene is in anti-sunward directions. In a low-altitude circular orbit and from the surface, the observational cadences would, respectively, be hourly and biweekly. LunaSOX satellites also carrying *in situ* space environment instruments could integrate into a network of orbital platforms for space weather monitoring and communications relay to far-side surface lander and permanent base sites, e.g., for low-frequency radio cosmology and detection of exoplanet magnetospheres.

KEYWORDS

heliophysics, solar corona, Moon, solar eclipse, solar wind

1 Introduction

One-half a century after the 7–19 December 1972 astronaut lunar landing mission of Apollo 17, the next high frontier of human exploration in the solar system for the 2023–2032 era of the present heliophysics decadal survey remains the Moon, its surface and local space environments, and cislunar to translunar space. The Moon's 60-R_E geocentric orbit takes it

from the deep magnetotail of Earth's magnetosphere to spend most of its time in the solar wind upwind of the magnetosphere in the local interplanetary environment. As such, the Moon is a target for solar wind plasma and energetic particle interactions and a stable surface and orbital platform for heliophysical observations of the Sun, its corona, the solar wind, and the geospace environment. Increasing cadences of robotic and human lunar missions will provide many potential missions of opportunity for heliophysics from the Moon, by the Moon, and of the Moon. This work extends our earlier white paper (Cooper et al., 2022) submitted to the ongoing heliophysics decadal survey.

Total solar eclipses by the Moon, as observed from Earth during recorded history (Golub and Pasachoff, 2010) and before, have long been events of great interest and sometimes fearful portents. Worldwide, they measure the passage of our lives at irregular cadences and provide only infrequent glimpses of the solar corona, at solar minimum a million times or fainter than the full Sun. Our co-author Professor Shadia Habbal (University of Hawaii Manoa), also leading on her own white papers (Habbal et al., 2010a; Habbal et al., 2022), made a distinguished career of observing many total eclipses as supported by her "Solar Wind Sherpas" (https://project.ifa.hawaii.edu/solarwindsherpas/) including our co-author Dr. Benjamin Boe (UHM). Altogether, Habbal observed 18 total eclipses, some under cloudy conditions, during 1995–2021. The late Prof. Jay Pasachoff (Williams College) famously logged 74 annular, partial, or total eclipses during 1959–2022. Co-author Dr. Edward C. Sittler Jr. scientifically observed the eclipses of 2017 in Idaho and 2019 in Chile (Sittler and Sittler, 2019). Our lead author Dr. John F. Cooper less scientifically observed the "Great European" eclipse of 1999 and the "Great American" eclipse of 2017 and expects to see the 2024 North American eclipse, but only in spirit the eclipse of 2078 from near his native city and future eternal abode of Savannah, Georgia. In the following sections, we propose, for the Artemis[1] generation and beyond, far more frequent solar eclipse observations at higher angular resolution and brightness sensitivity from the lunar orbit or surface at cadences of not years but hours to days to weeks.

An example of high spatial and spectral resolution of the inner corona is given in Figure 1 for the 1 August 2008 eclipse (Habbal et al., 2010b). Despite the 10^{-9} $B_{\odot}$[2] background of scattered atmospheric light at totality, details of coronal stream density and differential temperature structures are sharply visible. Of particular interest are the interactions between colder material in prominence from the photosphere and hotter adjacent material in coronal steamers. Another published work (Druckmüller et al., 2014) shows the inner details of small-scale structures such as smoke-like rings, faint nested expanding loops, expanding bubbles, and twisted-helical structures that can only be resolved at present with wideband observations shielded from the far brighter solar disk by the Moon. The radial expansion of the solar wind enlarges these emergent[3] features as drivers of interplanetary and geospace activity at 1 AU. In the past, only the SOHO LASCO C1 coronagraph (Brueckner et al., 1995) would have covered this region of the inner corona until instrument failure in 1998, but these faint features could not have been resolved by C1 due to internal light scattering. Solar eclipses by the Moon, whether from the vantage points of Earth or with higher resolution from the lunar orbit, are presently the only way to detect these white-light features. Moving outward at 2–4 $R_{\odot}$ per hour (400–800 km/s), these features could be tracked at bihourly cadences from the low-altitude lunar orbit.

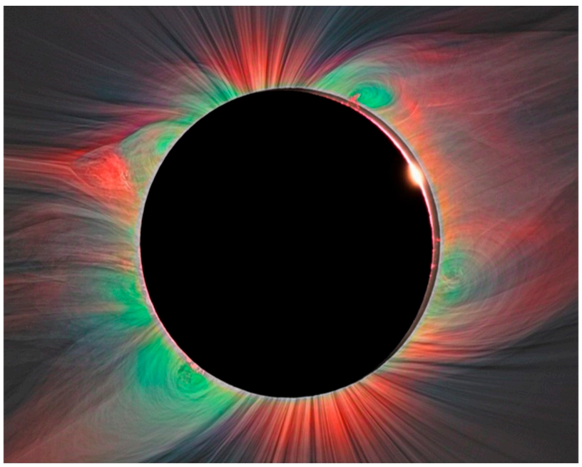

FIGURE 1
Multi-spectral composite image of the solar corona for the 2013 eclipse.: White for continuum and red and green for coronal emission lines of Fe XI and Fe XIV, respectively. Source: S. R. Habbal.

Lunar occultation of the solar disk, again from Earth or the Moon, uniquely enables the tracking of density structures via resonantly excited forbidden line emissions out to several solar radii (Habbal et al., 2013; Boe et al., 2022), well beyond the ~1.7 $R_{\odot}$ range of ultraviolet observations. In the absence of Earth's atmospheric light background, we might expect to extend such observations at least down to the 10^{-12} $B_{\odot}$ sensitivity of the LASCO C3 coronagraph beyond 4 $R_{\odot}$ and out to the 10 $R_{\odot}$ perihelia of the Parker Solar Probe (PSP) for comparison with *in situ* solar wind measurements from the PSP. As discussed in the following sections, this sensitivity is also the upper limit for local light scattering from the local lunar dust environment and is adopted for the present work.

A program of heliophysics observatories from, by, and of the Moon has the advantage of expanding mission-of-opportunities in the present decade and beyond from the increasing launch opportunities of the lunar human exploration program, also including lunar missions preparatory for later human exploration

1 Artemis is the presently ongoing NASA Moon-landing program, while all-upper-case ARTEMIS (Section 3) refers to two robotic spacecraft, P1 and P2, now in orbit at the Moon.

2 $B_{\odot}$ is the full unattenuated solar brightness at integrated apparent magnitude m-26.74 averaged over the solar disk of solid angle 6.80×10^{-5} sr as viewed from 1 au. Our assumed lunar brightness threshold of 10^{-12} $B_{\odot}$ is equivalent to the brightness of a star with integrated magnitude m+3.26 as averaged over a totally dark sky background of the same solid angle from 1 au as the solar disk. Resolving only the diffraction-limited size $(0.682 \text{ arcsec})^2$ of a point source with a telescope of aperture D = 20.3 cm (8 inches) yields a stellar magnitude threshold of mag+19.41 against the lunar background and m+22.73 with respect to integrated starlight as a lower limit from lunar orbit. In practice, a minimum signal/noise ratio of 10 at 2.5 magnitudes brighter than the threshold would be advisable for point source detection. From Earth's surface, the limiting apparent magnitude m = 7.5 + 5 log10(D) of the same telescope is mag+14.04. At these magnitudes, there are tens of millions to tens of billions of stars visible against the 10^{-12} $B_{\odot}$ lunar background.

of Mars in the following decade. Among the instrumentation of these missions could be multi-purpose telescopes with objectives spanning the heliophysics, planetary, astrophysics, and/or Earth science disciplines of NASA and other international space programs. At minimum, a sensitive solar corona telescope in the lunar orbit could explore the lunar atmospheric, dust, and zodiacal light foregrounds of observations for the solar corona.

Arguably the most important, but sometimes controversial, eclipse observation of the 20th century (Dyson et al., 1920), later confirmed by observers of other eclipses (Texas Mauritanian Eclipse Team, 1976) and by reanalysis of the 1919 photographic plates (Harvey, 1979), led to the confirmation of a key prediction for Einstein's theory of general relativity by measurement of the predicted maximum 1.75-arcsec deflection of starlight by the Sun's gravity. Higher-resolution confirmations (Will, 2014) of general relativity have come from radio measurements of quasars (1 in 10^4) and from Doppler measurements of Cassini spacecraft telemetry (1 in 10^5). At a nominal angular resolution of 10 microarcsec for 15th visual magnitude stars over a 7-year mission, the European Space Agency's GAIA astrometric spacecraft (de Bruijne, 2005) will resolve Einsteinian deflections to one part in 2×10^5 even far from the Sun. LunaSOX cannot offer improvements over these other techniques for general relativity verification but may have other astrophysical applications, e.g., lunar occultations of binary-star (Richichi et al., 1996; Wlasuk, 2000) and exoplanet (Richichi, 2003) systems with larger lunar surface telescopes.

A solar planetary objective could be the continuing search for small asteroids called vulcanoids with an expected zone of stability at 0.07–0.21 au (15–45 $R_\odot$), an upper limit at 99.7% confidence (Steffl et al., 2013), with no objects being greater than 5.7 km in diameter and no more than 76 objects above 1 km. Orbits of smaller objects are thought to be unstable on solar system time scales. Sun-grazing and sun-diving comets with respective perihelia <3.45 and 1.0 $R_\odot$ (Jones et al., 2018) could also be followed closer to the Sun than currently possible with heliospheric imagers of the type used for previous vulcanoid searches. Cometary and vulcanoid nuclei would only be seen as bright point objects in reflected sunlight, but comet tails and perhaps vulcanoid gas and dust clouds might be resolved. Finally, but perhaps most importantly, there is the critical planetary defense objective of searching for potentially hazardous objects with perihelia inward of Earth's orbit and normally hidden from view by the solar glare; these objects can otherwise only be seen above the local horizon in twilight before dawn and after sunset using Earth telescopes looking through challenging atmospheric seeing conditions and growing skylight pollution.

The primary science value discussed here for heliophysics of the Sun would be the enhanced resolution and far higher cadence of observations for small-scale spatial and temperature structures in the inner solar corona that could potentially be extended into the outer corona to 10 $R_\odot$, beyond the current 1.7 $R_\odot$ limit for UV imaging and 4 $R_\odot$ limit for Earth-based visible eclipse observations. These would only be snapshots in time from single orbital or surface observatories at such resolutions, but the time coverage could be expanded in the lunar orbit by a fleet of smallsats, each carrying, e.g., a 0.2 m diameter telescope providing arcsec spatial resolution, 700 km = 0.001 $R_\odot$ at the Sun, as routinely used for ground-based solar eclipse observations from Earth. From the lunar surface, a 2.4 m telescope like the Hubble Space Telescope (HST) would offer 0.04 arcsec resolution (40 km at the Sun) but only at biweekly cadences. That cadence could in theory (if not practically) be increased by siting the HST-size telescope in the lunar orbit. Larger lunar surface telescopes could biweekly offer corresponding finer resolution but would require mitigation against contamination by dust, e.g., by usage of entirely enclosed optical systems.

Continuous time coverage, e.g., for space weather forecasting, might be achievable with the PROBA-3 dual-satellite approach (see Section 6) as reapplied at L1 or the heliocentric orbit but not with lunar occultation from the lunar orbit. A possible exception would be a satellite continuously tracking the corona over the lunar limb from an Earth–Moon Lissajous orbit, although this option has not yet been studied by us. A solar-powered version of the latter could not operate in the lunar umbral shadow (total eclipse) region for longer than several hours, limited by chemical battery power, but longer operations could be sustained in the penumbral shadow region of partial eclipse or by nuclear battery power in the umbral region.

Eckersley and Kemble (2017) were granted a European patent for a trajectory concept transiently following the lunar shadow with unspecified spaceborne coronagraph and spacecraft in elliptical, parabolic, or hyperbolic orbits around Earth. Compared to their approach, the Lissajous orbit would require minimal propulsion energy for maintenance within the orbit but would require transits between the inner L1 and outer L2 Lissajous orbits to track the lunar shadow. Bartoněk et al. (2022) recently proposed another approach to viewing solar eclipses by the Moon with a small satellite in the low Earth orbit to remove the atmospheric interference problem but still only at the semi-annual cadence of eclipses also viewable from the ground. Greater orbital stability of observational spacecraft is suggested for usage of Earth as the solar occulter (Bernadini et al., 2022) but at the cost of loss in resolution by observing the corona through Earth's atmosphere.

In the following sections, we extend the scope of potential LunaSOX missions and measurements beyond the original concept of Habbal et al. (2013) and discuss technical requirements for solar coronagraphy from and by the Moon. Compared to the LunaSOX approach, relevant details are given for non-lunar approaches with other spaceborne telescopes. Any satellites in lunar orbits, including LunaSOX, could potentially be used for *in situ* space environment measurements as we also discuss. Finally, we offer our concluding assessment of the LunaSOX approach, its possible programmatic implementations, and its potential contributions to a network of space weather and communications relay satellites supporting Artemis-related activities on the Moon.

2 Science objectives

We address the science objectives and questions for a LunaSOX mission by first reviewing those for the Parker Solar Probe (PSP) as defined by Fox et al. (2016) and then identifying the remaining gaps in science coverage not filled by the PSP or other missions. The following PSP objectives as quoted from that paper are relevant to LunaSOX observations:

PSP.1: "Trace the flow of energy that heats and accelerates the solar corona and solar wind.

1a. How is energy from the lower solar atmosphere transferred to and dissipated in the corona and solar wind?"

The PSP particularly focuses on exploring *in situ* the region of solar wind flow below 20 $R_\odot$ during over 920 hours spread over many perihelion approaches during 2020–2025 of the primary mission. The spacecraft ultimately approaches the Sun just within 10 $R_\odot$ in the region of solar wind heating and acceleration. Early solar probe concepts called for a 4-$R_\odot$ perihelion, and therefore, the PSP does not cover the origination region of the ≤500-km/s slow solar wind characteristic of equatorial streamer belts. Figure 12 in the work of Fox et al. shows for the origination of the fast solar wind U ~ 800 km/s the expected speeds of 200 km/s at 2 $R_\odot$, 400 km/s at 4 $R_\odot$, 500 km/s at 5 $R_\odot$, 600 km/s at 10 $R_\odot$, and 700 km/s at 14 $R_\odot$, the latter at the expected transition from Alfvén wave speed V_A > U to V_A < U, beyond which the solar wind is no longer bound by solar magnetic fields and in bidirectional communication via Alfvén waves with the lower corona. The PSP actually first crossed this magnetic boundary at 18.8 $R_\odot$ and, thereafter, found to be variable in solar distance. The PSP also discovered transient switchbacks in the magnetic field (Mozer et al., 2020) that are rotational in structure and originate from Alfven wave activity, also contributing to solar wind heating and acceleration.

The first science question for the PSP and LunaSOX is whether the energy flow driving the solar wind occurs originally from Alfvénic turbulence rising upward from the granulated photosphere, from nanoflares at photospheric bright point convergences of magnetic flux, from reconnection of coronal magnetic fields, or from combinations thereof. Heat flow can be inferred from mapping coronal temperature and density gradients to the limits of telescope resolution, 1 arcsec in Figure 1 for white light with a 0.2 m aperture telescope but only 6 arcsec with smaller telescopes for narrow-band measurements of coronal ion emission lines. Even so, the interfaces of colder and hotter materials are clearly resolved. However, the PSP has no capability to map such emissions remotely, and there is presently no other capability to map these emissions through the inner and outer coronas out to 10 $R_\odot$ and beyond. Early in the SOHO mission, the LASCO C1 coronagraph mapped coronal line emissions in the inner corona but failed in 1998, and in any case, it did not have sufficient brightness sensitivity to continue such measurements into the outer corona. The eclipse observations from Earth provide only few minutes of observations at semiannual cadence for the time domain of coronal temperature and density evolution. The LunaSOX approach offers the prospect of hourly to daily to biweekly cadence with extended times up to 2 hours for each eclipse interval observed from and by the Moon.

PSP.2: "Determine the structure and dynamics of the plasma and magnetic fields at the sources of the solar wind. 2a. How does the magnetic field in the solar wind source regions connect to the photosphere and heliosphere? 2b. Are the sources of the solar wind steady or intermittent? 2c. How do the observed structures in the corona evolve into the solar wind?"

The PSP occasionally provides single-point measurements of the *in situ* magnetic field and plasma flow environment near and beyond 10 $R_\odot$ with additional context provided by the PSP (Vourlidas et al., 2016) and other coronal imagers including on the Solar Orbiter, SOHO, and STEREO spacecraft. Intermittency of sources and connections to the corona and the heliosphere are difficult to determine without continuous measurements in the space and time domains. As yet, there is little capability to measure magnetic fields from the inner to the outer corona inward of the PSP perihelion. Only models provide views of continuous connections from photospheric magnetic fields and flows to the outer corona.

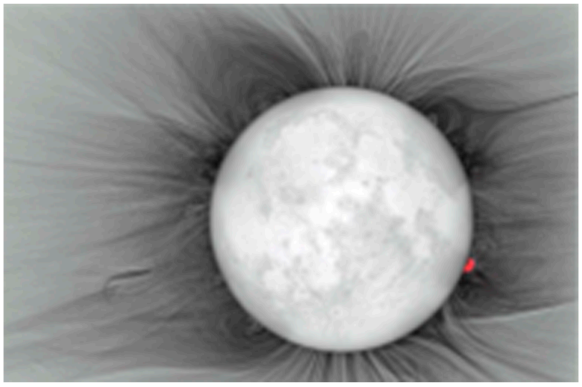

FIGURE 2
White light negative (black features are brightest) image of the total solar eclipse on 11 July 2010 (Habbal et al., 2011). Near side of the Moon lit by earthshine is shown. Red feature is prominence in Hα. Source by permission: S. R. Habbal.

In contrast, the wideband white light image in Figure 2 very clearly shows the directions and complexity of coronal magnetic fields and plasma flows directly off the solar limb, open at the poles and closed within bases of the equatorial streams, and with small-scale structures indicative of local turbulence. With a 0.2 m telescope in the lunar orbit, the spatial resolution at the solar limb would be 500 km, similar to the 10^3 km scale of photospheric granulation underlying the corona, but with larger telescopes in the lunar orbit or at the lunar surface, the smaller-scale 10^2 km features related to photospheric bright points between granules would be resolved. In 1-G coronal magnetic fields, the 50 m gyroradius scale of cyclotron wave turbulence from 1 keV protons would be resolved with a 10 m telescope from the lunar surface. Longer eclipse times from the lunar orbit enable extended tracking of all features in the time domain. Greater brightness resolution down to ≤$10^{-12}B_\odot$ from the lunar orbit also extends the radial range of tracking for large and small features beyond the 4-$R_\odot$ limit of Earth-based ground eclipse observations to the 10-$R_\odot$ PSP perihelion and beyond. Polarimetric measurements of the strong Fe XIII coronal line at 1,074.7 nm (Habbal et al., 2001) have been used to measure radial and non-radial components of the coronal magnetic fields. The He I line at 1,083.0 nm could also be used to measure the magnetic field via polarization from the quantum mechanical Hanle effect (Raouafi et al., 2016).

PSP 3: "Explore mechanisms that accelerate and transport energetic particles. 3a. What are the roles of shocks, reconnection, waves, and turbulence in the acceleration of energetic particles? 3b. What are the source populations and physical conditions necessary for energetic particle acceleration? 3c. How are energetic particles transported in the corona and heliosphere?"

The superheated populations of coronal plasma particles to MK temperatures apparently provide the source reservoirs for more energetic particles from acceleration by magnetohydrodynamic shocks associated with small- to large-scale flares and with coronal

mass ejections (CMEs). However, neither the PSP nor other spaceborne instruments can track energetic particle flows through the inner and outer coronas inward from 10 $R_\odot$. High-resolution ultraviolet and X-ray imaging can, however, be used to associate the acceleration regions of enhanced photonic emission to locations of local plasma heating from LunaSOX multi-spectral imagery. For example, the RHESSI spacecraft (Lin et al., 2002) operated from Earth's orbit as a NASA Small Explorer mission through early 2018 and provided 2–7 arcsec X-ray resolution comparable the visible-band imagery of Figure 2. On future missions, the X-ray resolution could be increased to 0.1 arcsec (Dennis et al., 2012) using a formation flying technique for complementarity to larger LunaSOX telescopes. Solar radio bursts (Pick and Vilmer, 2008) from electron acceleration can also be imaged by radio antenna arrays at Earth, e.g., the Very Large Array (VLA), and correlated to activity in LunaSOX coronal images.

3 LunaSOX mission concept

This mission concept generally covers any scenario in which a cislunar (<60 R_E), lunar, or translunar (>60 R_E) orbital satellite or a lunar surface platform is used to image the faint solar corona at brightness 10^{-6} to $\leq 10^{-12}$ $B_\odot$ at heliocentric distances of 1–10 + $R_\odot$ and beyond, while the 1-$B_\odot$ solar disk is totally or partially occulted by the lunar limb from the perspective of the observing satellite or surface platform. In principle, LunaSOX could be a single solar-powered satellite with a combination of chemical and ion propulsion systems that passes through all possible orbital phases en route from cislunar/translunar/Lissajous to the eccentric lunar orbit, low-altitude orbit, and even to landing on the lunar surface. Or, it could be a constellation of satellites that simultaneously operate, each in different orbital or surface phases, to assure more continuous time and spatial coverage of the corona at optimal spatial and spectral resolutions. Or, it could be the tasking of a larger lunar surface telescope facility for pre-sunrise and post-sunset observations.

The solar corona observations are herein assumed to be of primary interest for heliophysics from and by the Moon, but there could be other instruments for remote and *in situ* measurements dependent on the mission's interdisciplinary scope, also including heliophysics of the Moon. For example, a LunaSOX satellite could also carry a suite of magnetic field, plasma, plasma wave, neutral gas, energetic neutral atom, and/or energetic particle sensors for lunar space weather and surface space weathering applications in the solar wind and Earth's magnetotail. Constituents of the lunar atmosphere (e.g., Na and K; Killen et al., 2021; Leblanc et al., 2022; other species; Poppe et al., 2016) from solar wind sputtering and meteoritic impacts could be studied in solar eclipse from the lunar orbit and surface, also including in the ultraviolet for some atmospheric species that cannot be imaged from Earth surface telescopes. A UV-capable telescope could also be used to image Earth's hydrogen geocorona (Spann et al., 2007); the Apollo 16 lander crew first deployed in 1972 a surface UV telescope to image stars and Earth (Carruthers, 1973). A separate solar coronagraph with an external or internal occulter could be used for more continuous space weather observations at lower resolution. Biweekly lunar surface observations of the rising and setting solar corona would likely be only a small part of surface telescope facility operations but could be invaluable due to higher coronal resolution of smaller-scale processes for a large telescope.

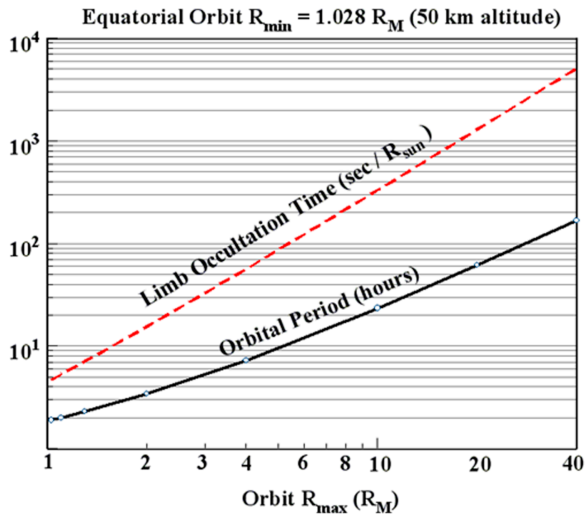

FIGURE 3
Rate (seconds/solar radius) of apparent rise/setting of the Sun (red curve) at lunar limb varies with period (black curve) and eccentricity of the lunar orbit with fixed periselene at a 50 km altitude and variable aposelene on the horizontal axis. The spacecraft orbit is simplified to be coplanar with the centers of the Moon and Sun. Source by permission: Habbal et al. (2013).

Common to all mission phases would be "by the Moon" occultation of the solar disk by the lunar limb which has an irregular altitude scale of ±8 km from surface topography as globally determined to meter resolution by the Lunar Orbiter Laser Altimeter (LOLA) (Barker et al., 2016) on the Lunar Reconnaissance Orbiter. Above the local topographic horizon, our assumed black space background (Section 4) is 10^{-12} $B_\odot$, 1,000 times lower than available for ground-based solar eclipse observations at totality from Earth. Assuming that the solar disk is fully occulted below the lowest topography, the lunar limb would have variable illumination up to 10^{-10} $B_\odot$ by earthshine, least at full Moon, anti-sunward from Earth, and most at sunward new Moon. A sufficiently narrow field of view (FOV) of the solar corona telescope is required to image only above the limb and avoid internally scattered light from earthshine and any un-occulted part of the solar disk when in the penumbral region. Three-axis control of the telescope platform attitude, and/or a moveable Sun filter, would be required to avoid telescope sensor damage from imaging the un-occulted solar disk when not performing disk-occulted coronal observations.

The cadence for solar eclipses by the Moon with respect to a satellite orbit coplanar with the Moon and Sun is dependent on the orbital period and eccentricity (Figure 3). The orbital periods are about 1 day in a 1 × 10 R_m orbit and 2 hours in the lowest-altitude circular orbits. At the lunar limb, as observed from the satellite, the Sun consecutively rises or sets every 12 h in the eccentric orbit and every hour in the circular orbit. The rising and setting times for the full solar disk (1 $R_\odot$) are 5 min and 5 s, respectively. Therefore, the full corona at 1–10 $R_\odot$ rises or sets over 45 min and 45 s for these two orbital examples. Greater orbital eccentricity gives longer

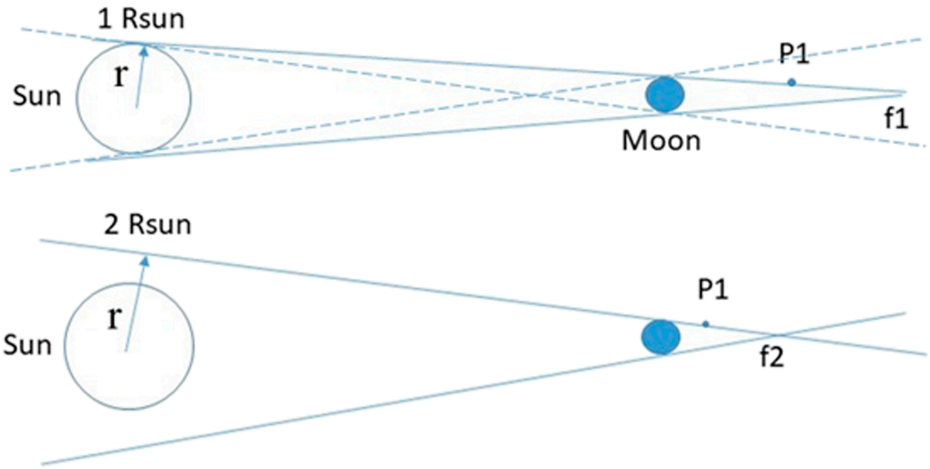

FIGURE 4
Positions for the P1 spacecraft at the edge of full lunar shadow cones (solid lines) for a solar disk at 1 $R_\odot$ (top) and at 2 $R_\odot$ (bottom) in the inner corona. The cone apexes are at points f1 and f2, respectively. The Sun + corona is occulted at $r \leq 1\ R_\odot$ and $r \leq 2\ R_\odot$, respectively, with respect to P1. By similar triangles, $r/(A+f) = R_m/f$ where A is the Sun–Moon distance (here assumed to be constant at 1 AU), f is the Moon–apex distance, and R_m is the Moon radius. f is also computed from the Selenocentric Solar Ecliptic (*X*-axis from the Moon toward the Sun and *Z*-axis northward perpendicular to ecliptic) coordinates of P1, from which r is then determined. Any coronal point at a radial solar distance greater than r is then visible from P1. The Moon's umbra for total eclipse is the part of the shadow cone between the Moon and the apex point. Two dashed lines in the top panel define the lunar penumbral region of partial solar eclipse, in which case the apex point is sunward of the Moon.

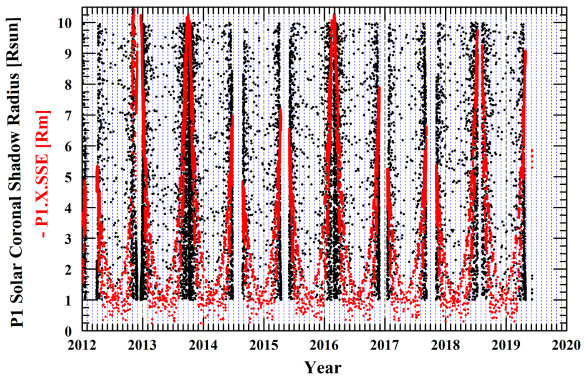

FIGURE 5
Computed coronal distance r values (black) at 1–10 $R_\odot$ from ARTEMIS P1 ephemeris for 2012–2019. Each point represents a time interval of a few minutes and may or may not be part of a longer consecutive observation sequence, the longer observation intervals being in the denser clusters of points. In red are the anti-sunward P1 distances at all times from the Moon along the Sun–Moon *X*-axis in Selenocentric Solar Ecliptic (SSE) coordinates. The anti-sunward values of X for P1 position in eclipse are negative, so we show only values with -X > 0. A time-extrapolated ephemeris for the satellite and the Moon at time intervals ~1 s would be required to more accurately compute eclipse times for short- and long-duration eclipses, hourly to daily. For observations at the lowest coronal altitude, further precision on occultation timing can be obtained by coupling the satellite ephemeris to maps of lunar limb surface topography.

dwell times for each eclipse observation but at a lower cadence. In comparison, totality times for Earth surface solar eclipses are a few minutes at a far lower semiannual cadence. For a lunar surface observatory near the equator, the full corona rises or sets in 4.7 h at a cadence of once every 14.8 days, nearly tracking at the corona the outward flow of the slow solar wind.

Real-world examples of selenocentric eccentric orbits for a future LunaSOX mission are available from the archived ephemeris data at the NASA Space Physics Data Facility (http://omniweb.gsfc.nasa.gov/) for the ARTEMIS (Acceleration, Reconnection, Turbulence, and Electrodynamics of the Moon's Interaction with the Sun) P1 and P2 satellites (Sweetser et al., 2011) in eccentric equatorial orbits from June–July 2011 through the present. These two satellites orbit in opposite directions around the Moon. There is precession of the major orbital axes relative to the sunward direction due to the Earth–Moon system's motion around the Sun. Figure 4 illustrates the geometry and defines the calculation for a spacecraft P1 being at the edge of the lunar umbral shadow cone of full eclipse for a coronal distance r from the center of the Sun. The shadow of the solar disk to 1 $R_\odot$ extends behind the Moon (top panel) to the apex point f1. The corona is partially visible to P1 for limited azimuth angles in a plane perpendicular to the Sun–Moon line for all solar distances greater than r in the corona. The spacecraft would have to be at f1 to observe all azimuth angles of the corona for given values of r. Figure 4 also illustrates the penumbral shadow cone in which the solar disk is partially visible to P1, and the f1 point would then be sunward of the Moon.

Using only the ARTEMIS P1 orbit, there would be many opportunities for solar eclipse observations, as shown in Figure 5. On the vertical axis, each black point indicates the minimum observable radial distance in the corona from the lunar orbit position of P1, from which the corona is observed beyond that distance at the Sun. Also shown by values of the red points on the plot's vertical axis are P1 distances from the Moon in lunar radii along the -X anti-sunward axis. Vertically uniform time gaps in the eclipse events occur when the aposelene axis is temporarily oriented outside of the

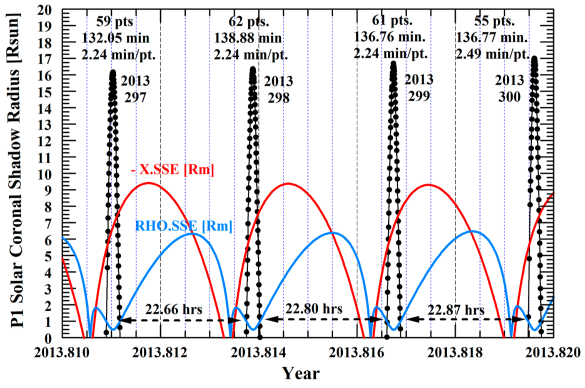

FIGURE 6
Expanded view of four consecutive eclipse scans (black points) from Figure 5 for days 297–300 of 2013 in time intervals of high eclipse point density. Red and blue curves denote P1 satellite distances in R_m at all times, respectively, down the -X SSE axis and for RHO = $\sqrt{Y^2 + Z^2}$ perpendicular to that axis. Eclipses occur only at P1 when -X > 0 and RHO <1.

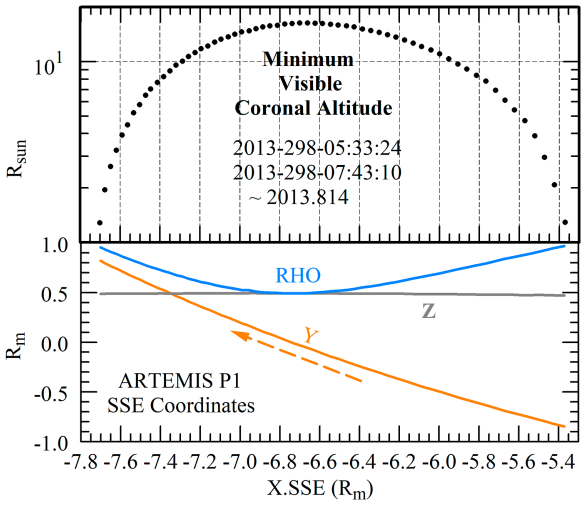

FIGURE 7
Upper panel: minimum visible coronal altitude in solar radii ($R_\odot$) vs. P1's X.SSE coordinate in lunar radii (R_m) of the 2 h continuous eclipse on day 298 of 2013 from Figure 6. Lower panel: Moon-centered Y (orange), Z (gray), and RHO (blue) *versus* X SSE coordinates of P1 during the eclipse. Note the vertical log scale on the upper panel and the vertical linear scale on the lower.

shadow cone, as occurs in two of every three precession cycles for the P1 orbit. Together, these data show that P1 eclipses occur more frequently and over longer time intervals when the orbital aposelene axis is toward the anti-sunward hemisphere with only sporadic rates of shorter eclipses for other orientations. Figure 6 shows a blowup of the highest density data for four eclipse sequences, each 2 hours long and separated by 23 h, on days 297–300 of 2013. Figure 7 shows the minimum coronal altitudes for all SSE coordinates during the day-288 eclipse. The orbit of a satellite could be controlled by ion propulsion to continue the Sun-synchronous orbit at this cadence or else lower the aposelene for higher cadences.

4 Technical requirements

4.1 Spacecraft orbit

The first requirement for LunaSOX operations is, of course, that the spacecraft must be in an orbit providing frequent opportunities for lunar limb occultation of the solar disk so that the far fainter corona will be easily visible. The eccentric equatorial orbits of ARTEMIS P1 and P2 and the low-altitude polar orbit of the Lunar Reconnaissance Orbiter would enable the daily and hourly cadence observations of the corona, respectively. A Sun-synchronous orbit in the Moon's dawn–dusk plane would have no solar occultations and be useless for coronal science, except if the solar telescope had its own external or internal occulting system, e.g., like LASCO C1, to provide 24/7 observations when higher-resolution and sensitivity observations requiring occultations are not required. In this case, a LunaSOX spacecraft would require sufficient maneuverability to transition between synchronous and non-synchronous orbits as required for different phases of science operations, as could be performed (see the following) with a solar-powered ion propulsion system. The NASA Lunar Orbital Platform–Gateway (Dandouras et al., 2023) will occupy a near-rectilinear halo orbit (NRHO) at lunar altitudes of 3,200 × 70,000 km with an orbital period ~6.5 days and a 90° polar inclination. The NHRO is designed for maximum visibility to Earth for communications and to the Sun for solar power and only rarely goes into solar eclipse, so it would not itself be useful for solar occultation observations. The gateway could, however, provide data relay services to all lunar orbiting spacecraft and surface facilities, including those supporting LunaSOX science.

4.2 Coronal brightness sensitivity and lunar dust

In lunar eclipse, an orbital telescope's sensitivity to coronal brightness would have a lower limit determined in part by the scattered light foreground from lunar atmospheric dust. Early suggestions of a detectable lunar exospheric dust environment came from visual observations made by astronauts on the Apollo command modules (McCoy, 1976) using cameras on these spacecraft (MacQueen et al., 1973; McCoy, 1976) and using cameras on Surveyor landers (Norton et al., 1967; Bohlin, 1971). The controversial question has been whether these observations showed a distinct low-altitude band from dust levitated off the surface, were confused with coronal streamers, zodiacal light, or else originated from instrumental scattered light. In two works, Glenar et al. (2011, 2014) respectively reanalyzed Apollo camera and Clementine star tracker images to set limits on lunar horizon glow and densities of exospheric dust. Although glow contributions from dust were confirmed for the Apollo imagery, there was no dust layer detection above a noise limit ~1–2 × 10^{-12} $B_\odot$ from the Clementine images.

Glenar et al. (2011) suggested a model in which meteoroidal impacts could transiently generate clouds of dust that then repeatedly interacted with the surface via saltation to generate higher dust densities at lower altitudes below 20 km and within 100 km of the local terminator. The impact-generated dust at high altitude would otherwise not be able to account for the Apollo observations. Apollo landings and takeoffs could have been sources. At 10 km altitude, the direct measurements (Horanyi et al., 2015; Szalay and Horanyi, 2015) by the Lunar Dust Experiment (LDEX) on the Lunar Atmosphere and Dust Explorer (LADEE) gave upper limits two orders of magnitude lower in density for micron-size particles compared to what would be required for the Apollo observations. The LADEX data did show an asymmetrical cloud of lunar dust with the highest densities toward the dawn hemisphere where maximum rates of meteoroid impacts were expected. A low-lying dust band was also not found by observations of far-ultraviolet scattered light (Feldman et al., 2014) with the LAMP instrument on the Lunar Reconnaissance Orbiter (LRO).

For now, we adopt the lunar dust brightness limit 10^{-12} $B_\odot$ from the work of Glenar et al. (2014) as the threshold for coronal observations from the lunar orbit. Even if the dust below the 20 km altitude was a more significant scattered light source, this would only compromise coronal viewing below 1.35 $R_\odot$ as observed by a LunaSOX orbiter from 7 $R_\odot$ anti-sunward of the Moon. Facing away from the Moon, Earth, and Sun, the integrated starlight background is much lower at 5×10^{-14} $B_\odot$ (Lang, 1980; Howard et al., 2020), allowing tracking of CMEs above that lower limit out to 67 $R_\odot$ (1 au = 215 $R_\odot$) by Howard et al.'s calculation. Above 10^{-12} $B_\odot$ from the lunar orbit, the CMEs would remain visible out to 15 $R_\odot$. With much higher resolution and sensitivity than the Clementine star tracker, a LunaSOX orbital telescope could observe in eclipse both the solar corona and exospheric dust to better determine the coronal brightness threshold.

4.3 Spacecraft operations, imaging, and spectroscopy

For maximum orbital flexibility in terms of cadence of eclipses *versus* duration of each eclipse, LunaSOX could use a combination of solar and battery power and electric ion propulsion. Ion propulsion operation outside of observational intervals would allow adjustment of orbital parameters for lower cadence and longer eclipses or for higher cadence and shorter eclipses. The maximum battery time in eclipse must, of course, be greater than the longest eclipse time of about 2 hours as per Figures 6, 7, and the present battery limit of 4 hours for the two ARTEMIS spacecraft in eclipse would be more than sufficient. The eclipse durations are longest when aposelenes of highly eccentric (e.g., 1×10 R_m) orbits are anti-sunward and shortest when in the dawn, sunward, and dusk directions. Orbital eccentricity and altitude control the hourly to daily cadence of eclipses, highest in the lowest-altitude circular orbit and lowest for the increasingly eccentric orbits.

An extremely important requirement is that internal solar telescope sensors sensitive to the faint coronal light must never view the 1.0-$B_\odot$ solar disk directly or otherwise be heated beyond their nominal temperature ranges by near-Sun pointing when not in eclipse. This requirement must be met with some combination of spacecraft attitude control, telescope and/or solar panel articulation, telescope internal filter design, and thermal design. The eccentricity-determined cadence of eclipses will drive the required response rate of the spacecraft and telescope systems for transition into and out of eclipses. This rate then determines the minimum coronal altitude of observation since the shortest transition interval must always occur when viewing closest to the Sun. For example, a spacecraft attitude slew time of 1 min would preclude any coronal observations from the lowest lunar altitude, as per Figure 3, if the telescope pointing was not separately controlled. It would likely be faster to rotate the telescope's internal filter wheel than to realign the entire spacecraft, but for continuous sunward pointing of the telescope aperture, there could then be thermal issues. The solar telescope filter wheel also requires rotation during eclipses for transitions between filters covering different coronal emissions, narrow and broad band.

The Solar Wind Sherpas use many telescopes on the ground from Earth to enable simultaneous observations in different wavelength bands within and outside the emission lines, the latter to determine continuum emission for subtraction from the total emission. A constellation of lunar orbiters with similarly capable telescopes would be required for the same approach from the Moon, or there might be two similar telescopes on each orbiter, one looking within and the other away from an emission line, then both transitioning in sequence to other filters for different lines. Another approach could be wideband imaging via a common entrance aperture and primary mirror, followed by beam splitting into multiple optical paths, each having their dedicated filters and detectors, so that several coronal lines could be observed simultaneously. Here, trades are required between spatial and spectral resolutions, time resolution vs. data volume, other spacecraft resources, and overall mission budget as optimized for differing observation goals between studies of small and large coronal structures and between steady-state and more transient processes.

The Solar Wind Sherpa observations of solar eclipses do not require high precision in telescope pointing since points in the images are co-registered to elements of the images such as streamers and bright background stars. How this would apply to LunaSOX observations is to be determined, in that only a limited ~180° angular segment of the corona is observed in a single observation at orbital distances <10 R_m from the Moon. The projected solar diameter at the lunar limb from 7 R_m anti-sunward is 114 km (0.54°), the same diameter as the lunar craters Gamow and Hevelius. If one had no knowledge of lunar topography, the total 16 km altitude variance of the lunar limb as observed from a typical LunaSOX distance of 7 R_m (Figure 6) projects to a coronal altitude range of 0.3 $R_\odot$ at the Sun, so registration of coronal points to the Moon would be more problematic.

With lunar topographic knowledge, the timing of rising and setting for the Sun relative to the LunaSOX spacecraft and the lunar limb can be predicted more precisely. The global topography of the Moon at a 60 m scale near the equator, and a smaller scale toward the poles, has been determined from co-registration of LOLA data from the LRO with terrain imaging data from the Japanese Kaguya/SELENE spacecraft (Barker et al., 2016). There is also a 100 m scale global topography product (Scholten et al., 2012) from stereographic imaging with the LRO Wide Angle Camera (WAC). More precise maps (Barker et al., 2021) have been created with LOLA data down to 5 m/pixel and Narrow Angle Camera (NAC)

images to 0.5 m/pixel in polar regions where solar illumination modeling (Tong et al., 2023) defines permanently shadowed regions for water ice deposits and adjacent sites with high illumination for Artemis surface solar power. A limiting factor in surface position resolution is uncertainty in spacecraft track position, down for the LRO to 1 m vertically and 50 m cross track when LOLA data are used (Zuber et al., 2010). In comparison, the ARTEMIS P1 and P2 positions can be determined with only radio tracking to 3 m at periselene and 24 m at aposelene, and we assume similar values for a LunaSOX orbiter.

Conservatively taking 100 m as the available lunar limb topography resolution for a future LunaSOX orbital spacecraft, we compute the projected altitude uncertainty range at the corona from LunaSOX at 7 R_m anti-sunward to be 0.002 $R_\odot$ with respect to a LunaSOX 0.2 m telescope pixel size of 0.7 arcsec = 0.0007 $R_\odot$ (41 m at the lunar limb) and the total lunar topographic range of 0.3 $R_\odot$ (16 km at the lunar limb). This could allow the coronal image points to be registered at 100 m pixel precision to the imaged lunar limb and the LOLA topographic map without precision pointing knowledge by the LunaSOX spacecraft. Dependent on the local limb topography within the telescope field of view, LunaSOX could image from the orbit through deep lunar valleys on the limb to small points in the lower corona down to 1.002 $R_\odot$.

Now, we compare the topographic uncertainty to the angular range of diffraction at any local point on the limb. For a distant point-like source imaged near the limb edge from Earth, the angular precision for separation of double stars is 20 milliarcsec (mas) (Wlasuk, 2000), which corresponds to a local lunar limb altitude of 37 m as seen from Earth. As viewed from Earth, the first five Fresnel peaks, varying from significantly first to negligibly last, are located within this altitude range (Böhm-Vitense, 1989). The altitude zone of these peaks is less than the limb topographic uncertainty and far less than the topographic amplitude of 8 km. The limb height of the border for each diffractive zone can be estimated from $h = (nd\lambda)^{1/2}$ where n is the zone number, d in meters is the observer distance from the limb, and λ = 550.0 nm is the typical wavelength (Verroi et al., 2008). For d = 60 R_E from Earth and 7 R_m for LunaSOX anti-sunward from the Moon, the fifth (n = 5) borders are at 32.4 m and 5.8 m, respectively, so the border location in the latter case for LunaSOX orbital observations is well within the topographic uncertainty. The maximum amplitude (n = 1) peak is within only 2.6 m (44 mas from 7 R_m) in local limb altitude. Scattering of sunlight off of large topographic features, and streaming sunlight between such features as from Baily's Beads (Baily, 1836) during total solar eclipses, will be far more important than diffraction light emission from the local limb edge. This is why it will be critical to include lunar topography data in the planning of the innermost corona observations.

As helpfully suggested by our reviewers, we can further apply equation (1) from the work of Landini et al. (2015) to determine the diffractive reduction from full Sun brightness after sunset behind the lunar limb with respect to the vantage point of LunaSOX at d = 7 R_m anti-sunward of the Moon. Scaling to the inverse square of dλ for λ = 550 nm, the minimum diffracted irradiance at LunaSOX would be 10^{-14} $B_\odot$, consistent with the low limb heights of diffractive rings as computed previously and not requiring any further reduction by instrumental occultation systems. In comparison, the formation flyer dual spacecraft approach of PROBA-3/ASPIICS (Section 5) offers an external occulter reduction of 10^{-4} $B_\odot$ at the imaging plane center (Aime, 2013; Figure 5 of the work of Landini et al., 2015).

The orbital dynamics limit the available exposure times for successive imaging during each eclipse interval. During the 2 h continuous eclipses shown in Figure 6, there would be ample time for multiple long exposures to repeatedly image and track motions of the fainter outer corona to 10 $R_\odot$ and beyond. The shorter intervals of eclipses at a low lunar altitude would be better suited for higher-cadence snapshot exposures to image the brighter innermost corona. Ideally, there could be a constellation of spacecraft in different circular to eccentric and equatorial to polar orbits for simultaneous coverage of different regions and time scales of the expanding corona. The constellation could also make other important measurements of the lunar space weather environment expanding those presently conducted by the two still-operational ARTEMIS spacecraft.

A minimum LunaSOX goal would be to reproduce the spatial and spectral resolution of the Sherpa observations, while doing these at much higher hourly to daily to biweekly cadences and at higher brightness sensitivity, from and by the Moon. Habbal et al. (2011) described their longest focal length telescope as a Ritchey–Chrétien type with 203 mm (8 inch) diameter and 1,624 mm focal length, giving an angular resolution of 1 arcsec in a 1.23^0 x 0.82^0 (~1^0x1^0) field of view. One degree from Earth, or the from the Moon at its average distance from the Sun, is 3.7 $R_\odot$ at the Sun. Centered on the solar disk, this view includes the 360° corona at 1.0–1.85 $R_\odot$, so multiple images must be taken to fully cover the corona out to ~4 $R_\odot$, the maximum extent of the ground-based observations as limited by sky brightness at totality. Exposure times varied from 0.002 to 2 s. Narrow-band 0.5-nm interference filters in the visible range were used for the following seven coronal lines: Hα (656.3 nm), Fe IX (435.9 nm), Fe X (637.4 nm), Fe XI (789.2 nm), Fe XIII (1,074.7 nm), Fe XIV (530.3 nm), and Ni XV (670.2 nm). These filters see 0.04% of the emission outside the bandpass at 300–1,100 nm. Multiple pairs of telescopes were used to image simultaneously on and off each line. Wideband measurements for white light images were performed at 400–650 nm.

For a LunaSOX flight telescope (Table 1), a similar focal length could be achieved with a folded light path as used in the SOHO LASCO C1 coronagraph (Brueckner et al., 1995) but without the need for an internal occulter and a Lyot stop (Lyot, 1939). In eclipse from and by the Moon, there would be no internal light scattering within the telescope from full Sun illumination, so we expect far greater brightness sensitivity down ≤10^{-12} $B_\odot$ in the lunar exospheric gas and dust environment above the occulting limb. Optionally, the same optics as in C1 could be used for full-time viewing of the corona, C1 always being pointed toward the Sun, whether or not the Moon blocks the field of view, and the solar disk being occulted internally except when in eclipse below the lunar limb.

Since not only the solar disk but also at least half the corona would be blocked by the Moon from the LunaSOX vantage point, the ~1^0x1^0 = 13.7 $R_\odot^2$ field of view for a 0.2 m telescope would focus on the visible half of the corona. A mosaic of overlapping images could be taken to either completely cover the visible corona out to the desired limiting corona altitude, e.g., 10 $R_\odot$, to concentrate on a particular angular sector or altitude range or to follow in time the radial and/or angular evolution of a coronal structure. For eclipse

TABLE 1 Summary of parameters for spaceborne coronagraphs.

Mission	Coronagraph or telescope	Occulter [1]	Bands[2]	Resolution (arcsec)	FOV ($R_\odot$)	Cadence (min–hr)	Integration time (s)	Dates
SOHO[3]	LASCO C1	INT LY	Na I, Fe XIV, Ca XV, Fe X, orange, Hα, WL, FP	5.6	1.1–3	≤1 h image downlink time	22 CCD readout	1996–1998
	LASCO C2	EXT INT LY	Blue, orange, light red, dark red, Hα, clear	11.4	1.5–6.0	≤1 h	22	1996–2025
	LASCO C3	EXT INT LY		56	3.7–30	≤1 h	22	
STEREO A[4]	SECCHI-COR1	INT LY	WL	3.75	1.5–4	8 min	11	2007–present + ?
	SECCHI-COR2	EXT INT LY	WL	14.7	2.5–15	15–60 min	15	
Solar Orbiter[5]	METIS	INV INT LY	WL	10.7 (20)	1.5–3.0 to 2.6–5.5	11 min	1–20	November 2021 + 7 (+3) years
PROBA-3[6]	ASPIICS	FF EXT INT LY	Fe XIV, He I D3, WL	2.8 (5.6)	1.2–3			2024 + 2 years
Aditya-L1[7]	VELC	INV LY	Fe XIV, Fe XI, Fe XIII, WL	2.5	1.05–3			2023 + 5 years
PUNCH[8]	Narrow Field Imager (NFI)	EXT	WL	11.4 (C2)	6–32	8 min	22–48	October 2024 + 2 years
SWFO-L1[9]	Compact Coronagraph (CCOR-2)	EXT IFoVC	WL	65	3.0–23.5	15 min	30[12]	February 2025 w/IMAP[13] + 5–10 years
GOES-U[9]	CCOR-1			33	3.7–18.7	15 min	30[12]	April 2024 + 15 years
Vigil-L5[10]	CCOR			96	2.7–25	5 min	30[12]	≥2029 + 10 years
LunaSOX[11]	Ritchey–Chrétien Telescope	LUN	Hα, Fe IX, Fe X. Fe XI, Fe XIII, Fe XIV, Ni XV, WL	0.7	1.002–10+	1–12 h (orbit) or 14 days (surface) per 180° coronal view	0.002–2 s	LOI[14] + ≥ 13 years
	D = 0.2 m f/8.0				~(1°)[12] = 13.7 $R_\odot$[22] per image			

(Continued on the following page)

10.3389/fspas.2023.1163517

TABLE 1 (*Continued*) **Summary of parameters for spaceborne coronagraphs.**

Mission	Coronagraph or telescope	Occulter [1]	Bands[2]	Resolution (arcsec)	FOV ($R_\odot$)	Cadence (min–hr)	Integration time (s)	Dates
1. EXT = external; INV = inverted (open hole); INT = internal (Lyot spot); LY = Lyot stop; IFoVC = inner field of view cutoff at the image surface; FF = formation flying; LUN = lunar limb								
2. Bandpasses (nm): Fe IX (435.9), Fe XIV (530.3), Ca XV (564.9), He I D3 (587.7), Na I (589.0), Fe X (637.4), Ni XV (670.2), Fe XI (789.2), Fe XIII (1,074.7), Hα (656.2), WL—White Light (various), FP—Fabry–Perot Interferometer (resolution 0.059–0.104), blue (420–520), orange (540–640), light red (620–780), dark red (730–835), IR—infrared (860–1,050), clear (400–850)								
3. Brueckner et al. (1995)								
4. Howard et al. (2008). STEREO-B launched in October 2006 along with STEREO-A but regular communications and data ended in late 2014 with last contacts in 2016 and official end of recovery operations in 2018								
5. Fineschi et al. (2012)								
6. Vivès et al. (2009), Galy et al. (2015)								
7. Prasad et al. (2017), Seetha and Megala (2017)								
8. DeForest et al. (2022)								
9. https://www.nesdis.noaa.gov/next-generation/space-weather/swfo-instruments								
10. https://space.oscar.wmo.int/satellites/view/vigil_l5#inst-ccor_vigil								
11. Habbal et al. (2011). We assume here no occultation mechanism, internal or external, other than the lunar limb (LUN). Vantage point is in lunar orbit or on the surface. The different bands are taken on different telescopes and at different angular resolutions in the ground-based observations. LunaSOX could use a main 0.2 m telescope with co-aligned filter wheels to cover some or all of the listed bands and also multiple polarizations								
12. https://www.goes-r.gov/spacesegment/CCOR_key_Meas_chart.html. Integration (exposure per image) times assumed to be the same for all CCOR coronagraphs								
13. Co-launch with the Interstellar Mapping and Acceleration Probe (IMAP)								
14. LOI—Lunar Orbital Injection. ARTEMIS P1 and P2 have been in the lunar orbit for 13 years								

10.3389/fspas.2023.1163517

intervals up to 2 hours, there would be ample opportunity to cover the visible corona in different ways compared to the few-minute time span of eclipses observed from Earth. Different viewing programs can be scheduled for each consecutive eclipse interval separated by 1–12 h for orbital operations and 2 weeks for surface platforms. On-board processing could be used to identify evolving features of particular interest and automatically adjust the program scheduling during and between consecutive intervals. The LunaSOX approach has the advantage of flexible schedule viewing for each half-corona without the angular resolution and scattered light limitations of non-lunar coronagraphs always centered on the solar disk as discussed in the next section. Furthermore, a sufficient constellation of LunaSOX orbital and surface platforms could simultaneously view all radial and angular sections of the corona.

LASCO C1 also differed from the Sherpa telescopes by using a tunable Fabry–Perot (FP) interference filter to allow consecutive viewing of different coronal lines, their Doppler shifts with the coronal plasma velocity, and their local continua. According to Table III in the study of Brueckner et al. (1995), the FP-enabled spectral resolutions were from 0.059 nm for Ca XV (564.9 nm) to 0.104 nm for Hα (656.3 nm), each tunable by ~ 1 nm for flows of ±500 km/s. For each coronal line, a separate blocking filter was used to further remove emission outside the FP-defined bands.

On LunaSOX, the FP approach could cover selected coronal lines and also provide access to the resonantly scattered Na D-2 (589.0 nm) and K (769.9 nm) lines (Potter and Morgan, 1988) for lunar atmospheric gas measurements. Only upper limits are currently available for remote measurements from Earth (Flynn and Stern, 1996; Stern, 1999) of metallic atom species, some of these limits being well below the stoichiometric abundances expected from the lunar surface composition. Scattered lines for the missing elements and other species would be brighter and perhaps more detectable as observed from near the Moon than from Earth. UV spectroscopy from the lunar orbit and surface, not possible from ground-based Earth telescopes, could probe the atmospheric abundances of H, He, Al, Mg, O, H, Ar, Ne, and Mn. Earth atmospheric scintillations that potentially obscure velocity distributions of lunar exospheric neutrals would, of course, be absent in LunaSOX observations.

5 LunaSOX comparisons to non-lunar spaceborne coronagraphs

In Table 1 and the following discussion, we review characteristics of relevant past (LASCO C1), present, and future spaceborne coronagraphs for comparison to suggested LunaSOX capabilities. The physics of edge diffraction provides a clear advantage to LunaSOX occultation by the distant lunar limb compared to artificial external and internal occulters and Lyot stops in the coronagraphs. Note below, e.g., that most of the diffractive fringe reduction for PROBA-3/ASPIICS is performed internally in that coronagraph and not by the formation flying occulter spacecraft. As proposed here, the LunaSOX telescope would have higher angular resolution than the coronagraphs, better resolution of the inner corona (finally replacing the lost SOHO LASCO C1), and potentially better brightness sensitivity for the outer corona. LunaSOX could also have the advantage of being integrated into an Artemis-related lunar space weather and communications relay network with very high data transfer rates (Section 6) supporting higher resolution and more frequent imagery.

The ASPIICS coronagraph on the upcoming PROBA-3 (Project for On-Board Autonomy) mission is due for launch from India in 2023 and will utilize formation flying between two spacecraft, the Coronagraph Spacecraft (CSC) carrying ASPIICS and the Occulter Spacecraft (OSC) with an external occulter disk at distances up to 150 m from the CSC (Vivès et al., 2009). PROBA-3 will be in an inclined eccentric geocentric orbit and ASPIICS will be operational for 6 consecutive hours in each 19.7 h orbit around the 60,530 km apogee when CSC and OSC are aligned at a minimum gravity gradient for solar coronal observations. The two spacecraft are separated much more at the 600 km perigee to avoid collisions at the maximum gravity gradient. The 2-year mission is designed as a technology testbed for formation flying.

ASPIICS will image the corona beyond the OSC occulter at 1.2–3 $R_\odot$ with the addition of an internal occulter, Lyot stop, and filter wheel for six combinations of spectral pass band and polarization (Galy et al., 2015). The original design was for minimum 1.08 $R_\odot$ but diffractive vignetting and formation flying control error extended this limit to 1.2 $R_\odot$. In comparison, LunaSOX (Table 1) could image within the lunar limb topography down to 1.002 $R_\odot$. There are selectable ASPIICS measurements of coronal emission lines for Fe XIV, He I, and Fe X and for white light. Internal straylight specifications limiting sensitivity for white light extend from 1.6×10^{-7} $B_\odot$ at 1.1 $R_\odot$ to 1.0×10^{-11} $B_\odot$ at 2.7–4.0 $R_\odot$. In the latter radial range, the expected K-corona brightness is respectively (3.2–1.0)x10^{-9} $B_\odot$ compared to 1.6×10^{-7} $B_\odot$ at 1.1 $R_\odot$. The straylight background goes below the usual 1.0×10^{-9} $B_\odot$ totality level of ground-based eclipses beyond ~1.62 $R_\odot$. As mentioned previously, the OSC occulter provides a diffractive intensity reduction of 10^{-4} $B_\odot$ at the entrance aperture to ASPIICS compared to the scaled value 10^{-14} $B_\odot$ from the lunar limb into a LunaSOX telescope.

In 2023, India will also launch the Visible Emission Line Coronagraph (VELC) and other solar instruments on the Aditya-L1 mission to the Earth–Sun L1 orbit. The VELC (Prasad et al., 2017; Seetha and Megala, 2017) has some similarities to LASCO C1 with an internal occulter and a folded light path design. Like C1 and ASPIICS, VELC is intended to cover the inner corona at 1.05–3 $R_\odot$. There are one visible continuum channel, two narrow-band visible channels (FeXIV and FeXI), and one infrared channel (FeXIII). Different from C1, the narrow-band channels use a multi-slit blazed reflection grating to spectrally split the incoming light beam toward separate detectors. The image resolution is 2.5 arcsec/pixel (similar to ASPIICS) with spectral resolution 0.0065 nm for the Fe XIV line compared to 5.6 arcsec/pixel and 0.065 nm for C1. A scattered light analysis from VELC optics modeling (Venkata et al., 2017) found a coronal brightness sensitivity range at 1.06–3 $R_\odot$ of 2.3×10^{-8}–1.3×10^{-9} $B_\odot$, better than C1 and perhaps comparable to ground-based observations but not what could be achievable with LunaSOX at sub-arcsec angular resolution, local dust background $\leq 10^{-12}$ $B_\odot$, and a simpler light path without the need for internal occultation and Lyot stops.

There are other ongoing and future missions with solar coronagraphs that image white light at a much lower angular resolution than LunaSOX could and would not do visible line

spectroscopy. The Multi-Element Telescope for Imaging and Spectroscopy (METIS) is operational (Fineschi et al., 2012) on the Solar Orbiter with an inclined heliocentric orbit and perihelion at 0.28 au. The METIS images the solar corona in the visible and UV spectra with a combination of multilayer mirror coatings and spectral bandpass filters. The coronal field of view is 1.5–3.0 $R_\odot$ at perihelion and 2.6–5.5 $R_\odot$ at 0.5 au. The visible sensitivity is quoted as < 10^{-9} $B_\odot$ with an angular resolution of 20 arcsec.

The Compact Coronagraph (CCOR) (Gong and Socker, 2004; Gong et al., 2019) from the Naval Research laboratory is being developed for flight on multiple spacecraft: 1) Space Weather Follow On-Lagrange 1 (SWFO-L1) mission to L1 to observe 3.0–23.5 $R_\odot$ (https://www.nesdis.noaa.gov/next-generation-satellites/space-weather/swfo-instruments); 2) on the GOES-U mission to the geostationary Earth orbit to observe 3.7–18.7 $R_\odot$ (SWFO-L1 ibid); and 3) on the European Space Agency's Vigil-L5 (formerly Lagrange-L5) mission (European Space Agency, 2022) to L5 to observe 2.7–25 $R_\odot$. The CCOR combines an external occulter (EO) and an Internal Field of View Occulter (IFoVC) near the image sensor plane to minimize vignetting beyond 3 $R_\odot$. Angular resolutions >1 arcmin are given in Table 1. These compact coronagraphs are being developed for low-mass and low-power applications on space weather monitoring platforms to better track coronal mass ejections from different vantage points.

The four smallsats of the PUNCH (Polarimeter to UNify the Corona and Heliosphere) mission (DeForest et al., 2022) will launch in 2025 into low-altitude (620 km), polar, and dawn–dusk Sun-synchronous Earth orbits with one Narrow Field Imager (NFI) and three Wide Field Imagers (WFI), each smallsat carrying one of the four instruments. The NFI is a compact externally occulted coronagraph similar to LASCO C2 and covering 6–32 $R_\odot$. DeForest et al. (2022) did not state the NFI and WFI angular resolutions, but for C2 (Brueckner et al., 1995), this is 11.4 arcsec at 1.5–6.0 $R_\odot$. The WFIs are heliospheric imagers based on the STEREO-HI design (Howard et al., 2008) covering 18–180 $R_\odot$ and by design attenuating direct sunlight to 10^{-16} $B_\odot$, notably well below the level of an average starlight background.

Also still operating on STEREO-A are the two externally occulted Lyot coronagraphs (COR1 and COR2) of the Sun Earth Connection Coronal and Heliospheric Investigation (SECCHI), as documented by Howard et al. (2008). The same coronagraphs on STEREO-B operated in tandem with STEREO-A until 2014. The SOHO LASCO C2 and C3 coronagraphs (Brueckner et al., 1995) remain operational despite the loss of C1 in 1998. Further details are listed in Table 1.

All of these spaceborne coronagraphs share with LunaSOX the advantage of no limit on resolution from the atmospheric turbulence that limits Earth ground-based observers to a few arcsec. So far, only LunaSOX with a 20 cm or greater aperture would extend observations to the sub-arcsec domain for greater detail on origins and evolution of small coronal structures and their temperature distributions. In fact, there would be no limit on the size and resolution of LunaSOX orbital or surface telescopes other than from budget and other resources. Both PROBA-3/ASPIICS and Aditya-L1/VELC can partially replace the lost capability of LASCO C1 with multi-spectral imaging and 360° coverage of the inner corona. Only Aditya-L1 would provide continuous time coverage, although with some latency for transmission of the data back at Earth. If we instead conceive of LunaSOX as a constellation of equatorial and polar orbiters also supporting other science and acting as communications relays, then more continuous solar coverage would become available.

6 Comparison of data rates

Within a LunaSOX FOV ~1° × 1° at 0.7 arcsec resolution (Table 1) for each recorded image, there would be 26 million pixels. Each image is for white light-filtered by the selected bandpass and polarization on an internal filter wheel and/or Fabry–Perot interferometer, so there is only one image channel. Let each pixel readout of coronal intensity be losslessly compressed for transfer to 8 bits or 1 byte. At one image per second over typically two total hours in eclipse per day, this yields 190 GB. Imaging at sub-arcsec resolution with a larger telescope, and/or faster imaging occasionally even down to millisec intervals as for the ground-based total eclipse observations, could easily bring the data rate requirement up to several TB/day and even higher from multiple orbiters and surface platforms.

Orbital location within the Earth–Moon system is preferable for high-data rate operations. The Lunar Reconnaissance Orbiter now downlinks 0.5 TB/day from the total data transfer of multiple instruments to a Ka-band antenna network at White Sands Test Facility in New Mexico. At a higher data rate, White Sands receives 1.5 TB/day from the Solar Dynamics Observatory (SDO) in the Earth geosynchronous orbit. According to the ESA Satellite Missions Catalog (https://www.eoportal.org/satellite-missions/proba-3) entry for PROBA-3, the expected downlink rate to antenna facilities in Europe is 80 megabits/sec or 0.2 TB for 6 hours of observation per 19-h orbit. In the Earth orbit, the PUNCH maximum downlink rates will be 5 Mbps in the S band to 25 Mbps in the X band, 0.054–0.270 TB/day.

Laser communications test systems could support rates of 0.2–200 Gbps (2.8 TB/day–2.2 PB/day) for lunar and Earth orbital systems, respectively. These laser tests include the Lunar Laser Communications Demonstration (LLCD) on the Lunar Atmosphere and Dust Environment Explorer (LDEE) mission (Boroson and Robinson (2014), the TeraByte InfraRed Delivery (TBIRD) system on a NASA cubesat in the low-altitude Earth orbit, and the Orion Artemis II Optical Communications System (O2O) to operate onboard the crewed Orion spacecraft for the Artemis 2 lunar flyby mission, presently due for launch in November 2024. Petabyte per day relay systems in the lunar orbit could clearly support a large constellation of LunaSOX and other orbital and surface platforms performing both science and communication relay tasks in support of future Artemis missions.

Scheduling priorities for Earth ground antenna stations will always limit daily viewing opportunities and average data rates and increase data latency (delay in downlink of recorded data) for deep space missions operating far beyond the Earth–Moon system. The Aditya-L1 mission (Prasad et al., 2017) will return only 15 GB/day out of 0.25 TB/day in on-board data production, while SOHO continues with 2 GB/day going to the NASA Deep Space Network. In its 168-day inclined solar orbit at 0.28–0.91 au, the METIS coronagraph (Fineschi et al., 2012) on the Solar Orbiter downlinks 3.25 GB per orbit or 19.35 MB/day. The SECCHI

coronagraphs (COR1 and COR2) on STEREO-A (Howard et al., 2008) normally downlink 828 images per day or about 200 MB/day. In total, SECCHI can process 5,000 images per day from all its instruments and downlink more of these during special observation campaigns at a higher data rate. Since its launch in 2018, the Parker Solar Probe returned 3 TB of total data through 2022 or on average 0.8 TB/year = 2.2 GB/day.

7 *In situ* lunar ionosphere measurements

In situ exospheric ion measurements would be desirable since backgrounds tend to be less for neutrals, e.g., due to terrestrial contaminant outgassing from the spacecraft and instruments. The Neutral Mass Spectrometer on the lunar orbital LADEE spacecraft did find in ion mode (Halekas et al., 2015) the following exospheric ions with mass number in parenthesis: H_2^+ (2), He^+ (4), C^+ (12), O^+ (16), Ne^+ (20), Na^+ (24), K^+ (39), and Ar^+ (40), and for mass 28, either Si^+ or CO^+ or N_2^+. LADEE and earlier lunar missions had detected H_2^+, He^+, C^+, O^+, Na^+, Al^+, Si^+, K^+, Ar^+, Ca^+, and Fe^+. LADEE NMS detected water group ions, but these are thought to be from spacecraft vapor background and not of lunar origin. Benna et al. (2019) did report neutral water group neutrals (OH and H_2O) from NMS and correlated to interplanetary dust stream impacts releasing the water from the lunar surface as previously hydrated by solar wind interaction.

Spacecraft outgassing background is eliminated in measurements of eV–keV lunar exospheric ions by plasma ion spectrometers since the ions are first born far from the spacecraft after ionization in the neutral atmosphere and then picked up by the solar wind magnetic field and accelerated in the associated electric field. Habbal et al. (2013) briefly discussed these measurements. One challenge is to separate different ions of the same mass/charge M/Q, e.g., lunar exospheric atomic O^+ *versus* S^{++} and molecular CH_4^+ with all three ions having M/Q = 16 amu/charge, or solar wind $^4He^{++}$ vs. exospheric H_2^+. Considering the importance of lunar water and oxygen for Artemis *in situ* resource utilization, the relative abundances for the water group ions (H, O, OH, H_2O, H_3O, and O_2) would have high priority but remain undetermined thus far. These separations are particularly challenging when one ion has higher abundance than the others by orders of magnitude.

Many plasma spectrometers use electrostatic analyzers (ESAs) to determine energy/charge E/Q abundances. Ion mass spectrometers (IMSs) further utilize time-of-flight techniques to measure ion mass M as a function of E/Q. Saito et al. (2010) combined these techniques at the Moon to measure exospheric C^+, O^+, Na^+, K^+, and Ar^+ ions with their ion mass analyzer on SELENE/Kaguya, but the separation from neighboring ions was limited. Additional techniques to filter out more abundant ions, e.g., with tighter limits on ion velocity, and more precisely measure minor and trace ion abundances look promising and have been under development by co-author Sittler, including for an upcoming sounding rocket test with R. Mitchell (https://issuu.com/nasagsfc/docs/fall_2022_final_web_version.pdf/s/17253196) to measure precipitating suprathermal proton and oxygen ions within Earth's auroral zone. Mass scans may also be performed to search for minor ions. Combined analyses (Poppe et al., 2016) of the NMS gas and LDEX dust experiments on LADEE have advanced a joint understanding of exospheric and surface abundances. More knowledge of the exospheric neutral gas, ion, and dust environments of the Moon awaits the many potential civilian and commercial flight opportunities for improved instruments to become available during the Artemis human exploration era.

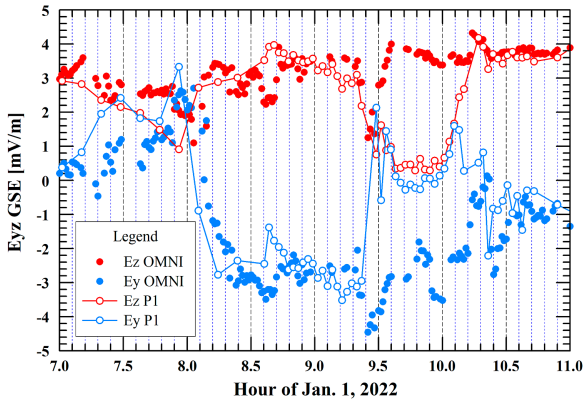

FIGURE 8
Convective electric fields in the Y (blue circles) and Z (red circles) GSE directions from the OMNI database (solid circles), as time shifted to Earth's magnetospheric bow shock and from the ARTEMIS P1 spacecraft (open circles) at the Moon for 1 January 2022.

The lunar ionospheric measurements would best be performed in conjunction with measurements for magnetic and electric fields, and for solar wind plasma flow, all these measurements are presently being performed by the ARTEMIS P1 and P2 spacecraft and potentially to be performed in various iterations of NASA's Lunar Orbital Platform–Gateway (Dandouras et al., 2023). Modeling of the ion trajectories for tracking back to ionospheric and surface source locations can be peformed with knowledge of the fields (Sarantos et al., 2012), but these are best determined at the Moon since the upstream solar wind is perturbed by the lunar ionospheric interaction and when the Moon is in the magnetotail of Earth's magnetosphere. In the lunar frame, there is a convective electric field E computable from the cross product -VxB of the vectors for the bulk solar wind flow V and the magnetic field B, all of which vary between the solar wind monitors (OMNI database: https://omniweb.gsfc.nasa.gov/) upstream of Earth's magnetosphere and in the local lunar environment (P1 and P2). The upstream and local electric fields are shown at 1 min time resolution during part of 1 day in Figure 8 for two vector components as computed from OMNI and P1 data. The upstream and local fields generally track each other with small deviations but greatly diverge when P1 enters the downstream wake of the Moon. In practice, it is unlikely that all variations of the fields and plasma around the Moon and upstream in the solar wind can be simultaneously measured, but a limited network of lunar space environment monitors could be used to constrain parameters to continuously update lunar ionospheric interaction models (Lipatov et al., 2018) providing globally computed maps of the fields and plasma.

8 Conclusion and discussion

Fifty-one years after the last Apollo Moon landing, heliophysics from, by, and of the Moon and other multi-disciplinary science can now be advanced in the current decade and beyond in conjunction with the Artemis human exploration program. We have discussed how a LunaSOX network of orbital and surface platforms could contribute to solar coronal science and other objectives in heliophysics, planetary science, astrophysics, and planetary defense. The current gap in high-resolution visible band coverage of the inner and outer coronas, since the 1998 demise of SOHO LASCO C1, could be filled beyond the semi-annual cadence of ground-based solar eclipse observations by 24 per year for a single surface platform to hundreds to thousands of observations per year from lunar orbital platforms. The vantage points looking over the sun-occulting lunar limb offer arcsecond and better diffraction-limited telescope observations without Earth's atmospheric seeing interference, without sky brightness background above an upper limit $\leq 10^{-12}$ $B_\odot$ on scattered light from lunar dust, and without need for external and/or internal instrument occultation and/or an internal Lyot stop to block out the diffractive fringe from the extremely bright solar disk. This limit is at least 1,000 times lower than Earth sky background at solar eclipse totality and could be even lower down to the integrated starlight background 5×10^{-14} $B_\odot$ if the scattered light contribution from atmospheric dust is much lower than the observational limit. The sharp cutoff at the lunar limb of 1-$B_\odot$ emission from the solar disk, with respect to a distant surface or orbital observer, is evident in this paper from simple diffraction analysis for occulter edges but is also obvious from sunlit images of Earthrise from the Apollo, Kaguya, and Lunar Reconnaissance Orbiter missions. Present knowledge of the lunar topography at 10 m resolution would allow precise determinations of sunrise and sunset times for each eclipse observation, enabling coronal viewing at lower solar altitudes, while avoiding near total solar eclipse, the Baily's beads and diamond ring (single bead) effects of visibility through valleys between lunar topographic features. It should also be noted that all annular eclipses, for which the solar disk edge is just visible from Earth above all of the lunar limb, result not at all from diffractive fringes but from occasions of greater distance of the Moon in an elliptical orbit at 57.6–63.6 R_E around Earth. The increased visible brightness sensitivity could extend coronal wideband and narrow-band observations outward beyond the present 4 $R_\odot$ limit to 10 $R_\odot$ or more, the domain to be covered *in situ* by minimum perihelia of the ongoing Parker Solar Probe mission.

At minimum, a versatile LunaSOX-type smallsat with solar electric ion propulsion, three-axis attitude control, and a 0.2 m diameter telescope with solar disk, wideband, narrow-band, and polarization filters could carry out eclipse by the Moon observations during the cislunar, translunar, and lunar orbit phases of the mission. This pathfinder mission could be supported by heliophysics Small Explorer funding and/or as a Mission of Opportunity tied to robotic and human exploration and habitation of the Moon and its space environment. MIDEX, moderate, and large-scale mission options could be pursued for constellations of lunar environment satellites performing both remote and *in situ* science, and for multi-disciplinary science, e.g., a larger lunar surface telescope also for stellar and exoplanet astrophysics.

There is also the interesting potential compromise of placing a more traditional Lyot coronagraph in the orbit around the Moon, or even moving an existing coronagraph spacecraft into the lunar orbit, as a hybrid LunaSOX platform. When not in eclipse, this platform could carry out continuous solar corona observations at the lower sensitivities of present spaceborne coronagraphs. In eclipse, the usual Lyot coronagraph limitation of internal scattered light background would go away for periodic observations at higher resolution and sensitivity.

An orbital network of lunar space weather spacecraft could also importantly provide communications relay and time-critical space weather updates to lunar far-side landers and permanent surface stations never otherwise in direct radio contact with Earth. For the same reason, the lunar farside is particularly attractive for radio astronomy, since commercial and military transmitters otherwise cause radio frequency interference (RFI) in surface and orbital astronomical receivers. In the search for extraterrestrial intelligence (SETI), for example, a far-side antenna receiver facility would not have to separate a true extrasolar signal from most of the cacophony of human transmissions. Burns (2021) described a lunar far-side program of cosmological radio observations for the highly red-shifted 21 cm emission from interstellar hydrogen in the early Universe and beginning with the Dark Ages Polarimeter PathfindER (DAPPER) lunar orbiter, now in development to collect data only on the farside, to be followed later by farside surface antennas. Burns also noted the potential farside astronomy application in the detection of radio emissions from extrasolar planetary magnetospheres, likely important as on Earth for shielding of habitable planetary environments against space weather effects that evidently stripped away most of the early atmosphere on Mars. Science from the Moon is also discussed in the context of the NASA Artemis program by Valinia et al. (2022).

Finally, surveys for potentially hazardous and other solar system objects moving against the relatively fixed stars may benefit by moving some operations from Earth's surface and orbital platforms to the lunar environment where there is not (yet) a growing cloud of many thousands of commercial satellites (e.g., SpaceX's Starlink constellation) transiently contaminating the natural starlight background (Barentine et al., 2023). These satellites are highly visible during prime twilight viewing times at Earth and contaminate a fraction of observations when some surveys critical for planetary defense are looking for objects closer to the Sun. For the same size of telescope, resolution and sensitivity would be much improved for telescopes operating from the Moon and not having to look up through the $\geq 10^{-9}$ $B_\odot$ scattered sunlight even at solar eclipse totality in Earth's atmosphere.

Our lead author closes for us by expressing his personal disappointment that a half-century after the Apollo missions, the same time span as his long postgraduate career now continuing into scientifically active retirement, the Moon and its space environment do not already bristle with a multitude of inhabited bases and robotic platforms advancing human science, technology, commerce, and understanding of the Cosmos. However, the lead author does not regret his alternate career path not taken in fusion energy research, which also 50 years later has not yet come to fulfillment with economical fusion power. After the Apollo landings, we have robotically explored all the planets of the solar system, including brief looks with New Horizons at Pluto and the Kuiper Belt, but

we do not yet live and work and play above the low Earth orbit. Human geospace, soon expanding to the Moon and its cislunar and translunar domains, still remains to be fully explored and inhabited, while Mars and elsewhere beyond geospace beckon to the more intrepid voyagers who, like Tennyson's Ulysses, seek newer worlds. There is still much to be done from and by and of the Moon, and we offer the LunaSOX multi-mission concept as one very doable, scientifically productive, and cost-effective pathway supporting heliophysics, lunar science, astrophysics, Earth science, and planetary defense objectives into the age of Artemis.

Data availability statement

The datasets presented in this study can be found in online repositories. The names of the repository/repositories and accession number(s) can be found as follows: The ARTEMIS P1-P2 ephemeris and solar wind datasets used in this white paper were provided online by the NASA Space Physics Data Facility (https://spdf.gsfc.nasa.gov/) and are directly available as part of SPDF's OMNIWeb database under "Moon Related Spacecraft" at https://omniweb.gsfc.nasa.gov/. The commercial software package PSI-Plot Version 10.5 from Poly Software International Inc. (http://polysoftware.com/) was used for data analysis and figure production. Solar Wind Sherpa eclipse images of the solar corona are available at the Hawaii Total Solar Eclipse Database (https://www2.ifa.hawaii.edu/SolarEclipseData/). Further details on LRO LOLA lunar topography datasets are available at the Geosciences node of the Planetary Data System.

Author contributions

JC led this research as a Senior Scientist Emeritus of the Heliospheric Physics Laboratory of NASA Goddard Space Flight Center. SH and BB provided inputs on instrumentation and science goals for ground-based solar eclipse observations. DS and VA advised on orbits and science operations of the ARTEMIS P1 and P2 spacecraft. LJ provided our data and science interface to the NASA Space Physics Data Facility. NP advised on instrument technology and development of the mission concept. ES advised on plasma ion instrumentation. RK advised on lunar exospheric measurements.

Funding

This work is an extended version of the LunaSOX community white paper submitted for the Decadal Survey for Solar and Space Physics (Heliophysics) 2024–2033. JF JC acknowledges support during his earlier NASA employment (2005–2021) for his project "Solar Wind Interaction with Lunar Exosphere and Surface," from which the LunaSOX mission concept first arose, from the NASA Lunar Advanced Science and Exploration Research (LASER) program. Further partial support for LunaSOX concept development came from two consecutive research teams of the NASA Solar System Exploration Research Virtual Institute (SSERVI): DREAM2—Dynamic Response of Environments at Asteroids, the Moon, and moons of Mars—and LEADER—The Lunar Environment And Dynamics for Exploration Research, respectively, led by W. M. Farrell and RK of the NASA Goddard Space Flight Center. SH and BB were supported by NASA and NSF grants to the University of Hawaii at Manoa.

Acknowledgments

The authors thank R. Howard at the Applied Physics Laboratory of Johns Hopkins University and C. Korendyke and D. McMullin at the Space Systems Research Corporation for providing background information on the LASCO C1 instrument.

Conflict of interest

The authors declare that the research was conducted in the absence of any commercial or financial relationships that could be construed as a potential conflict of interest.

Publisher's note

References

Aime, C. (2013). Theoretical performance of solar coronagraphs using sharp-edged or apodized circular external occulters. *Astron. Astrophys.* 558, A13. doi:10.1051/0004-6361/201322304

Baily, F. (1836). I. On a remarkable phenomenon that occurs in total and annular eclipses of the sun. *MNRAS* 4, 15–19. doi:10.1093/mnras/4.2.15

Barentine, J. C., Venkatesan, A., Heim, J., Lowenthal, J., Kocifaj, M., and Bará, S. (2023). Aggregate effects of proliferating low-Earth-orbit objects and implications for astronomical data lost in the noise. *Nat. Astron.* 7, 252–258. doi:10.1038/s41550-023-01904-2

Barker, M. K., Mazarico, E., Neumann, G. A., Smith, D. E., Zuber, M. T., and Head, J. W. (2021). Improved LOLA elevation maps for south pole landing sites: Error estimates and their impact on illumination conditions. *Plan. Sp. Sci.* 203, 105119. doi:10.1016/j.pss.2020.105119

Barker, M. K., Mazarico, E., Neumann, G. A., Zuber, M. T., Haruyama, J., and Smith, D. E. (2016). A new lunar digital elevation model from the lunar orbiter laser altimeter and SELENE terrain camera. *Icarus* 273, 346–355. doi:10.1016/j.icarus.2015.07.039

Bartoněk, J., Lazar, V., Malaník, P., Rydlo, Š., Láznička, T., Popela, R., et al. (2022). Low Earth orbit determination in small satellite mission proposal for corona observation of close solar surface region. *Acta Astron* 203, 202–213. in press. doi:10.1016/j.actaastro.2022.11.052

Benna, M., Hurley, D. M., Stubbs, T. J., Mahaffy, P. R., and Elphic, R. C. (2019). Lunar soil hydration constrained by exospheric water liberated by meteoroid impacts. *Nat. Geosci.* 12, 333–338. doi:10.1038/s41561-019-0345-3

Bernardini, N., Baresi, N., Roberto Armellin, R., Eckersley, S., Sarah, A., and Matthews, S. A. (2022). Trajectory design of Earth-enabled sun occultation missions. *Acta Astron* 195, 251–264. doi:10.1016/j.actaastro.2022.02.027

Boe, B., Habbal, S., Downs, C., and Druckmüller, M. (2022). The solar minimum eclipse of 2019 july 2. II. The first absolute brightness measurements and MHD model predictions of Fe x, xi, and xiv out to 3.4 $R_\odot$. *Astrophys. J.* 935, 173. doi:10.3847/1538-4357/ac8101

Bohlin, D. D. (1971). Photometry of the outer solar corona from lunar-based observations. *Sol. Phys.* 18, 450–457. doi:10.1007/BF00149067

Böhm-Vitense, E. (1989). *Introduction to stellar astrophysics*. Cambridge: Cambridge University Press.

Boroson, D. M., and Robinson, B. S. (2014). The lunar laser communication demonstration: NASA's first step toward very high data rate support of science and exploration missions. *Sp. Sci. Rev.* 185, 115–128. doi:10.1007/s11214-014-0122-y

Brueckner, G. E., Howard, R. A., Koomen, M. J., Korendyke, C. M., Michels, D. J., Moses, J., et al. (1995). The Large-Angle Spectroscopic Coronagraph (LASCO) visible light coronal imaging and spectroscopy. *Sol. Phys.* 162, 357–402. doi:10.1007/BF00733434

Burns, J. O. (2021). Transformative Science from the Lunar Farside: Observations of the dark ages and exoplanetary systems at low radio frequencies. *Phil. Trans. R. Soc. A* 379, 20190564. doi:10.1098/rsta.2019.0564

Carruthers, G. R. (1973). Apollo 16 far-ultraviolet camera/spectrograph: Instrument and operations. *Appl. Opt.* 12, 2501–2508. doi:10.1364/AO.12.002501

Cooper, J. F., Habbal, S. R., Boe, B., Angelopoulos, V., Sibeck, D. G., Paschalidis, N., et al. (2022). Heliophysics from, by, and of the moon in the age of Artemis: Lunar solar occultation explorer (LunaSOX). White paper submitted to the decadal survey for solar and space physics (heliophysics) 2024-2033. Available at: https://www.nationalacademies.org/our-work/decadal-survey-for-solar-and-space-physics-heliophysics-2024-2033.

Dandouras, I., Taylor, M. G. G. T., De Keyser, J., Futaana, Y., Bamford, R. A., Branduardi-Raymont, G., et al. (2023). Space plasma physics science opportunities for the lunar orbital platform – Gateway. *Front. Astron. Sp. Sci.* 10. in press. doi:10.3389/fspas.2023.1120302

de Bruijne, J. H. J. (2005). "*Accuracy budget and performances" in proceedings of the gaia symposium "the three-dimensional universe with gaia" (ESA SP-576)* C. Turon, K. S. O'Flaherty, and M. A. C. Perryman, ESA SP-576. Available at: http://www.rssd.esa.int/index.php?project=Gaia&page=Gaia_2004_Proceedings.

DeForest, C., Killough, R., Gibson, S., Henry, A., Case, T., Beasley, M., et al. (2022). "Polarimeter to UNify the corona and heliosphere (PUNCH): Science, status, and path to flight," in 2022 IEEE Aerospace Conference (AERO), USA, 5-12 March 2022 (Big Sky, MT), 1–11. doi:10.1109/AERO53065.2022.9843340

Dennis, B. R., Skinner, G. K., Li, M. J., and Shih, A. Y. (2012). Very high resolution solar x-ray imaging using diffractive optics. *Sol. Phys.* 279, 573–588. doi:10.1007/s11207-012-0016-7

Druckmüller, M., Habbal, S. R., and Morgan, H. (2014). Discovery of a new class of coronal structures in white light eclipse images. *Astrophys. J.* 785, 14. doi:10.1088/0004-637X/785/1/14

Dyson, F. W., Eddington, A. S., and Davidson, C. (1920). A determination of the deflection of light by the Sun's gravitational field, from observations made at the total eclipse of May 29, 1919. *Phil. Trans. Roy. Soc. Lond. A* 220, 291–333. doi:10.1098/rsta.1920.0009

Eckersley, S., and Kemble, S. (2017). *A Method of solar occultation*. European patent office, European patent 2 641 833 B1. Applied 20.03.2012, granted 18.10.2017 Bulletin 2017/42. url: Available at; https://patentimages.storage.googleapis.com/c2/5b/47/24e29c5f4e5ddb/EP2641833B1.pdf.

European Space Agency (2022). *Vigil mission objectives and payload description*, 5. European Space Operations Centre, Darmstadt, Germany.

Feldman, P. D., Glenar, D. A., Stubbs, T. J., Retherford, K. D., Gladstone, G. R., Miles, P. F., et al. (2014). Upper limits for a lunar dust exosphere from far-ultraviolet spectroscopy by LRO/LAMP. *Icarus* 233, 106–113. doi:10.1016/j.icarus.2014.01.039

Fineschi, S., Antonucci, E., Naletto, G., Romoli, M., Spadaro, D., Nicolini, G., et al. (2012). Metis: A novel coronagraph design for the solar orbiter mission. Proc. SPIE 8443, space telescopes and instrumentation. *Ultrav. Gamma Ray* 2012, 84433H. doi:10.1117/12.927229

Flynn, B. C., and Stern, S. A. (1996). A spectroscopic survey of metallic species abundances in the lunar atmosphere. *Icarus* 124, 530–536. doi:10.1006/icar.1996.0228

Galy, C., Fineschi, S., Galano, D., Howard, R. A., Kintziger, C., Kirschner, V., et al. (2015). Design and modelisation of ASPIICS optics, *Proc. SPIE 9604. Sol. Phys. Space Weather Instrum.* VI, 96040B. doi:10.1117/12.2188404

Glenar, D. A., Stubbs, T, J., Hahn, J. M., and Wang, Y. (2014). Search for a high altitude lunar dust exosphere using Clementine navigational star tracker measurements. *J. Geophys. Res. Plan.* 119, 2548–2567. doi:10.1002/2014JE004702

Glenar, D. A., Stubbs, T. J., McCoy, J. E., and Vondrak, R. R. (2011). A reanalysis of the Apollo light scattering observations, and implications for lunar exospheric dust. *Plan. Sp. Sci.* 59, 1695–1707. doi:10.1016/j.pss.2010.12.003

Golub, L., and Pasachoff, J. M. (2010). *The solar corona*. Cambridge, UK: Cambridge University Press.

Gong, Q., Gopalswamy, N., and Newmark, J. (2019). *Proc. SPIE 11116*, II, 111160F. doi:10.1117/12.2530408Innovative compact coronagraph approach for balloon-borne investigation of temperature and speed of electrons in the corona (BITSE)*Astronomical Opt. Des. Manuf. Test Space Ground Syst.*

Gong, Q., and Socker, D. (2004). Theoretical study of the occulted solar coronagraph. *Proc. SPIE 5526, Opt. Syst. Degrad. Contam. Stray Light Eff. Meas. Control*, 208–219. doi:10.1117/12.549275

Habbal, S. R., Boe, B., Haggerty, C., and Ding, A. (2022). A total solar eclipse earth-based mission: Multi-wavelength observations from land, sea and air to probe the critical middle corona, community white paper, 2024-2033 Solar and Space (Heliophysics) Decadal Survey. url: Available at: https://www.nationalacademies.org/our-work/decadal-survey-for-solar-and-space-physics-heliophysics-2024-2033.

Habbal, S. R., Cooper, J., Daw, A., Ding, A., Druckmüller, M., Esser, R., et al. (2010a). *Exploring the Physics of the Corona with total solar eclipse observations*. Community white paper, solar and space physics decadal survey (heliophysics), space science board. *Natl. Acad. Sci*. doi:10.48550/arXiv.1108.2323

Habbal, S. R., Druckmüller, M., Morgan, H., Ding, A., Johnson, J., Druckmüllerov, H., et al. (2011). Thermodynamics of the solar corona and evolution of the solar magnetic field as inferred from the total solar eclipse observations of 2010 July 11. *Astrophys. J.* 734, 120. doi:10.1088/0004-637X/734/2/120

Habbal, S. R., Druckmüller, M., Morgan, H., Scholl, I., Rušin, V., Daw, A., et al. (2010b). Total solar eclipse observations of hot prominence shrouds. *Astrophys. J.* 719, 1362–1369. doi:10.1088/0004-637X/719/2/1362

Habbal, S. R., Morgan, H., Druckmüller, M., Ding, A., Cooper, J. F., Daw, A., et al. (2013). Probing the fundamental physics of the solar corona with lunar solar occultation observations. *Sol. Phys.* 285, 9–24. doi:10.1007/s11207-012-0115-5

Halekas, J. S., Benna, M., Mahaffy, P. R., Elphic, R. C., Poppe, A. R., and Delory, G. T. (2015). Detections of lunar exospheric ions by the LADEE neutral mass spectrometer. *Geophys. Res. Lett.* 42, 5162–5169. doi:10.1002/2015GL064746

Harvey, G. M. (1979). Gravitational deflection of light. A re-examination of the observations of the solar eclipse of 1919. *Observatory*. Available at: https://articles.adsabs.harvard.edu/pdf. 99, 195–198.

Horanyi, M., Szalay, J. R., Kempf, S., Schmidt, J., Grün, E., Srama, R., et al. (2015). A permanent, asymmetric dust cloud around the Moon. *Nature* 522, 324–326. doi:10.1038/nature14479

Howard, R. A., Moses, J. D., Vourlidas, A., Newmark, J. S., Socker, D. G., Plunkett, S. P., et al. (2008). Sun earth connection coronal and heliospheric investigation (SECCHI). *Sp. Sci. Rev.* 136, 67–115. doi:10.1007/s11214-008-9341-4

Howard, R. A., Vourlidas, A., Colaninno, R. C., Korendyke, C. M., Plunkett, S. P., Carter, M. T., et al. (2020). The solar orbiter heliospheric imager (SoloHI). *Astron. Astrophys.* 642, A13. doi:10.1051/0004-6361/201935202

Jones, G. H., Knight, M. M., Battams, K., Boice, D. C., Brown, J., Giordano, S., et al. (2018). The science of sungrazers, sunskirters, and other near-Sun comets. *Space Sci. Rev.* 214, 20. doi:10.1007/s11214-017-0446-5

Killen, R. M., Morgan, T. H., Potter, A. E., Bacon, G., Ajang, I., and Poppe, A. R. (2021). Coronagraphic observations of the lunar sodium exosphere 2018 – 2019. *Icarus* 355, 114155. doi:10.1016/j.icarus.2020.114155

Landini, F., Bemporad, A., Focardi, M., Fineschi, S., Romoli, M., Pancrazzi, M., et al. (2015). Significance of the occulter diffraction for the PROBA3/ASPIICS formation flight metrology, *Proc. SPIE 9604. Solar Physics and Space Weather Instrumentation*, VI, 96040E. doi:10.1117/12.2187916

Lang, K. R. (1980). *Astrophysical formulae*. New York: Springer-Verlag, 572.

Leblanc, F., Schmidt, C., Mangano, V., Mura, A., Cremonese, G., Raines, J. M., et al. (2022). Comparative Na and K mercury and moon exospheres. *Sp. Sci. Rev.* 218, 2–56. doi:10.1007/s11214-022-00871-w

Lin, R. P., Dennis, B. R., Hurford, G. J., Smith, D. M., Zehnder, A., Harvey, P. R., et al. (2002). The reuven ramaty high-energy solar spectroscopic imager (RHESSI). *Sol. Phys.* 210, 3–32. doi:10.1023/A:1022428818870

Lipatov, A. S., Sarantos, M., Farrell, W. M., and Cooper, J. F. (2018). Effects of multiscale phase-mixing and interior conductance in the lunar-like pickup ion plasma wake. First results from 3-D Hybrid Kinetic Modeling. *Plan. Sp. Sci.* 156, 117–129. doi:10.1016/j.pss.2018.02.017

Lyot, B. (1939). The study of the solar corona and prominences without eclipses (George Darwin Lecture, 1939). *Mon. Not. R. Astron. Soc.* 99, 580–594. doi:10.1093/mnras/99.7.538

MacQueen, R. M., Ross, C. L., and Mattingly, T. (1973). Observations from space of the solar corona/inner zodical light. *Plan. Sp. Sci.* 21, 2173–2179. doi:10.1016/0032-0633(73)90191-8

McCoy, J. E. (1976). Photometric studies of light scattering above the lunar terminator from Apollo solar corona photography. *Proc. Lunar Sci. Conf.* Available at: https://articles.adsabs.harvard.edu/pdf. 7th, Vol. 1, pp. 1087 – 1112.

Mozer, F. S., Agapitov, O. V., Bale, S. D., Bonnell, J. W., Case, T., Chaston, C. C., et al. (2020). Switchbacks in the solar magnetic field: Their evolution, their content, and their effects on the plasma. *Astrophys. J. Suppl. Ser.* 246 (7pp), 68. doi:10.3847/1538-4365/ab7196

Norton, R., Gunn, J. E., Livingston, W. C., Newkirk, G. A., and Zirin, H. (1967). Surveyor 1 observations of the solar corona. *J. Geophys. Res.* 72, 815–817. doi:10.1029/JZ072i002p00815

Pick, M., and Vilmer, N. (2008). Sixty-five years of solar radioastronomy: Flares, coronal mass ejections and sun–earth connection. *Astron. Astrophys. Rev.* 16, 1–153. doi:10.1007/s00159-008-0013-x

Poppe, A. R., Halekas, J. S., Szalay, J. R., Horányi, M., Levin, Z., and Kempf, S. (2016). LADEE/LDEX observations of lunar pickup ion distribution and variability. *Geophys. Res. Lett.* 43, 3069–3077. doi:10.1002/2016GL068393

Prasad, B. R., Banerjee, D., Singh, J., Nagabhushana, S., Kumar, A., Kamath, P. U., et al. (2017). Visible emission line coronagraph on aditya-L1. *Curr. Sci.* 113, 613–615. doi:10.18520/cs/v113/i04/613-615

Richichi, A., Baffa, C., Calamai, G., and Lisi, F. (1996). The TIRGO lunar occultation program; summary of the 1985-1995 observations. *Astron. J.* 112 (6), 2786–2798. doi:10.1086/118221

Richichi, A. (2003). Lunar occultations of stars with exoplanet candidates. *Astron. Astrophys.* 397, 1123–1127. doi:10.1051/0004-6361:20021585

Sarantos, M., Hartle, R. E., Killen, R. M., Saito, Y., Slavin, J. A., and Glocer, A. (2012). Flux estimates of ions from the lunar exosphere. *Geophys. Res. Lett.* 39, L13101. doi:10.1029/2012GL052001

Scholten, F., Oberst, J., Matz, K.-D., Roatsch, T., Wählisch, M., Speyerer, E. J., et al. (2012). GLD100: The near-global lunar 100 m raster DTM from LROC WAC stereo image data. *J. Geophys. Res.* 117, E00H17. doi:10.1029/2011JE003926

Seetha, S., and Megala, S. (2017). Aditya-L1 mission. *Curr. Sci.* 113, 610–612. doi:10.18520/cs/v113/i04/610-612

Sittler, E. C., Jr., and Sittler, L. M. (2019). *Semi-empirical 2D model of the solar corona and solar wind using solar eclipse images: Progress report Solar and stellar magnetic fields: Origins and manifestations proceedings IAU symposium No 354* A. Kosovichev, K. Strassmeier, and M Jardine. doi:10.1017/S1743921320000551

Steffl, A. J., Cunningham, N. J., Shinn, A. B., Durda, D. D., and Stern, S. A. (2013). A search for vulcanoids with the STEREO heliospheric imager. *Icarus* 223, 48–56. doi:10.1016/j.icarus.2012.11.031

Stern, S. A. (1999). The lunar atmosphere: History, status, current problems, and context. *Rev. Geophys.* 37, 453–491. doi:10.1029/1999RG900005

Sweetser, T. H., Broschart, S. B., Angelopoulos, V., Whiffen, G. J., Folta, D. C., Chung, M.-K., et al. (2011). ARTEMIS mission design. *Sp. Sci. Rev.* 165, 27–57. doi:10.1007/s11214-012-9869-1

Szalay, J. R., and Horanyi, M. (2015). The search for electrostatically lofted grains above the Moon with the Lunar Dust Experiment. *Geophys. Res. Lett.* 42, 5141–5146. doi:10.1002/2015GL064324

Texas Mauritanian Eclipse Team (1976). Gravitational deflection of light: Solar eclipse of 30 June 1973 I. Description of procedures and final results. *Astron. J.* 81, 452–454. doi:10.1086/111906

Tong, X.-H., Huang, Q., Liu, S.-J., Chen, H., Wang, Y. Q., Xu, X., et al. (2023). A high-precision horizon based illumination modeling method for the lunar surface using pyramidal LOLA data. *Icarus* 390, 115302. doi:10.1016/j.icarus.2022.115302

Valinia, A., Grunsfeld, J. M., Hess, M. G., Green, J., Schier, J., Haas, J. P., et al. (2022). *Unique science from the moon in the Artemis era*. Hampton, Virginia: NASA Langley Research Center. NASA/TM–20220017053. NESC-RP-22-01729.

Venkata, S. N., Prasad, B. R., Nalla, R. K., and Singh, J. (2017). Scatter studies for visible emission line coronagraph onboard ADITYA-L1 mission. *J. Astron. Telesc. Instr. Syst.* 3, 014002. doi:10.1117/1.JATIS.3.1.014002

Verroi, E., Frassetto, F., and Naletto, G. (2008). Analysis of diffraction from the occulter edges of a giant externally occulted solar coronagraph. *J. Opt. Soc. Am. A* 25, 182–189. doi:10.1364/JOSAA.25.000182

Vivès, S., Lamy, P., Koutchmy, S., and Arnaud, J. (2009). ASPIICS, A giant externally occulted coronagraph for the PROBA-3 formation flying mission. *Adv. Sp. Res.* 43, 1007–1012. doi:10.1016/j.asr.2008.10.026

Vourlidas, A., Howard, R. A., Plunkett, S. P., Korendyke, C. M., Thernisien, A. F. R., Wang, D., et al. (2016). The wide-field imager for solar probe plus (WISPR). *Sp. Sci. Rev.* 204, 83–130. doi:10.1007/s11214-014-0114-y

Will, C. M. (2014). The Confrontation between general relativity and experiment. *Living Rev. Relativ.* 17, 4. doi:10.12942/lrr-2014-4

Wlasuk, P. T. (2000). *Observing the moon*. London: Springer-Verlag.

Zuber, M. T., Smith, D. E., Zellar, R. S., Neumann, G. A., Sun, X., Katz, R. B., et al. (2010). The lunar reconnaissance orbiter laser ranging investigation. *Space Sci. Rev.* 150, 63–80. doi:10.1007/s11214-009-9511-z